This is a preprint, the final version is subject to change, of the American Mineralogist (MSA)
Cite as Authors (Year) Title. American Mineralogist, in press.
(DOI will not work until issue is live.) DOI: http://dx.doi.org/10.2138/am-2017-5949

Revision #1

Iron partitioning in natural lower-mantle minerals: Toward a chemically heterogeneous lower mantle

Felix V. Kaminsky [1,*], Jung-Fu Lin [2]

[1]KM Diamond Exploration Ltd., West Vancouver, British Columbia, V7S 3J1 Canada

[2]Department of Geological Sciences, Jackson School of Geoscience
The University of Texas at Austin, Austin, TX, USA

Abstract

The concentrations of Fe, Al and Ni and their distributions were determined for all known natural assemblages of ferropericlase (*fPer*) and bridgmanite (*Bridg*), coexisting as inclusions in deep-mantle diamonds from Brazil, Canada, Guinea and South Australia. Based upon these data, it is likely that some areas within the deep lower mantle are iron-rich and differ markedly from a pyrolitic composition. In the lowermost lower mantle, *Bridg* is Al-rich and *fPer* is Ni-poor, witnessing the presence of a free metallic phase in the mineral-forming environment. The iron partitioning in the *Bridg* + *fPer* association ($K_D^{\text{Bridg-fPer}} = ([\text{Fe/Mg}]^{Bridg})/([\text{Fe/Mg}]^{fPer})_{at}$) in juvenile diamond inclusions is as low as 0.1-0.2. During ascent of the diamonds with their inclusions to the surface, the $K_D^{\text{Bridg-fPer}}$ eventually increases to values of 0.4-0.5 and even as high as 0.7.

* E-mail: felixvkaminsky@aol.com

The details of the element partitioning between natural *Bridg* and *fPer* in the lower mantle are as follows: iron in *Bridg* is ferrous Fe^{2+} in the A site, substituting for Mg^{2+}; almost all iron in *fPer* is ferrous Fe^{2+}; the share of ferric Fe^{3+} iron in *fPer* is $Fe^{3+}/\Sigma Fe$ = 8-12 at%; iron concentrations in both *Bridg* and *fPer* increase with depth (pressure), reflecting the increasing Fe content in the lower part of the lower mantle, different from that of a pyrolitic model. Al in *Bridg* is mainly in the cation site B and partly in the cation site A, in both cases substituting for Si, Mg and Fe with vacancy formation; and in the case of Al positioning into both B and A sites, a charge-balanced reaction occurs.

The natural samples show very diverse $K_D^{Bridg\text{-}fPer}$ values and elemental distribution that cannot be simply explained by our current understanding on alumina dissolution in *Bridg* and the spin transition of Fe^{2+} in *fPer*. These major differences between experimental results and observations in natural samples demonstrate the complex, inhomogeneous iron speciation and chemistry in the lower mantle.

Keywords: lower mantle, ferropericlase, bridgmanite, iron partitioning, pyrolite

Introduction

The Earth's lower mantle, based on a pyrolite compositional model, is believed to comprise three major mineral species, bridgmanite [$(Mg,Fe)(Si,Al)O_3$], ferropericlase [(Mg,Fe)O] and calcium silicate perovskite [$CaSiO_3$], that are gravitationally compressed near adiabatically. It has been proposed that these minerals are distributed homogeneously and have constant compositions, for the most part through the lower mantle, and thus contribute to continuous

46 features of the observed, one-dimensional seismic model of density, compressional wave
47 velocity and shear wave velocity (Dziewonski and Anderson 1981; Kennett et al. 1995).
48 Bridgmanite (*Bridg*) and ferropericlase (*fPer*) contain significant amounts of iron, whose
49 complex chemical speciation and electronic spin transitions can affect a broad spectrum of the
50 physical and chemical properties of the two major phases of the lower mantle (e.g., Irifune et al.
51 2010; Lin et al. 2013).

52 High *P-T* experiments along an expected mantle geotherm for a pyrolitic composition
53 demonstrated that the iron index, $fe = Fe/(Fe+Mg)_{at}$, of the pyrolitic lower-mantle *fPer* should be
54 0.12-0.27 (e.g., Wood 2000; Lee et al. 2004) or even lower, at c. 0.10 (Kesson and Fitz Gerald
55 1991). These results suggest that the iron chemistry of lower-mantle *fPer* may not vary
56 significantly. However, although a majority of the studied natural lower-mantle *fPer* grains
57 hosted within deep-diamond inclusions have $fe = 0.10\text{-}0.20$, more than 40 % of them vary in a
58 'forbidden' range with up to $fe = 0.62$, falling into the field of magnesiowüstite (e.g., Hutchison
59 1997; Kaminsky 2012); one of the analyzed samples has an iron index even as high as 0.9, which
60 is almost close to the end-member wüstite stoichiometry. Some *Bridg* grains, coexisting with
61 iron-rich *fPer*, also exhibit relatively high iron contents. The discovery of these iron-rich
62 ferropericlase and magnesiowüstite grains deviates from the traditional view of the pyrolitic
63 lower mantle composition that displays a homogenous iron chemistry and mineralogy, and points
64 to a much more complex chemistry of the lower mantle.

65 To elucidate the lower-mantle chemistry in these minerals, we have analyzed Fe, Ni and Al
66 contents and their distribution in all the currently known *fPer* + *Bridg* assemblages coexisting as
67 inclusions in natural diamonds from Brazil, Canada, Guinea and South Australia.
68

Review of experimental data

A number of experimental works on iron partitioning between *Bridg* and *fPer* in a laser-heated diamond anvil cell, subjected to relevant lower-mantle conditions of up to approximately 120 GPa, were performed over the last two decades. Almost all experiments modelled the suggested pyrolitic model of the lower mantle with the iron index, $fe = Fe/(Fe+Mg)_{at} = 0.05$-0.10. The only exception was the work performed by Tange et al. (2009) in a multianvil apparatus with sintered diamond anvils, in which the starting material was very different from pyrolitic and had $fe = 0.50$; it resulted in highly iron-rich association, *Bridg* with $fe = 0.16$-0.32 and *fPer* with $fe = 0.49$-0.92. The other studies have shown disparate results for the distribution of Fe in the various minerals (Fig. 1A). For example, while some demonstrated a positive correlation of the iron index between *Bridg* and *fPer* (0.070-0.234) (Katsura and Ito 1996; Kesson et al. 2002; Kobayashi et al. 2005; Murakami et al. 2005; Sakai et al. 2009); others found the opposite, a negative correlation (Irifune 1994; Kesson et al. 1998; Wood 2000; Irifune et al. 2010) (Fig. 1A). At $fe_{fPer} = 0.05$-0.20 for both trends, the positive correlation was obtained mainly in association with low-Fe *Bridg* ($fe = 0.010$-0.103), while the negative correlation was in association with high-Fe *Bridg* ($fe = 0.081$-0.167). There were, as well, experimental results showing variations in $fe_{Bridg} = 0.011$-0.077 virtually independently of fe_{fPer} (c. 0.10) (Auzende et al. 2008). The general trends (I and II) can be identified in a consolidated graph (Fig. 1A). The positive trend divides into two branches (trends Ia and Ib) with the same correlation but different values of fe_{Bridg}, which could be due to different pressure range examined. These experimental discrepancies remain unexplained.

Experimental evaluations of the partition coefficient of iron between *fPer* and *Bridg*

defined as $K_D^{Bridg\text{-}fPer} = ([Fe/Mg]^{Bridg})/([Fe/Mg]^{fPer})_{at}$ produce even more inconsistent results. The values of $K_D^{Bridg\text{-}fPer}$ vary from 0.04 to 0.9 (Fig. 1B). Some of the experiments have shown an increase of $K_D^{Bridg\text{-}fPer}$ with pressure (Irifune, 1994; Kobayashi et al. 2005; Sinmyo and Hirose, 2013), whereas others have demonstrated the reverse (Andrault 2001; Kesson et al. 2002; Murakami et al, 2005; Tange et al. 2009; Irifune et al. 2010), or have found no correlation between $K_D^{Bridg\text{-}fPer}$ and pressure (Guyot et al. 1988; Katsura and Ito 1996; Auzende et al. 2008). Specifically, the concentration of Al^{3+} in bridgmanite has been shown to significantly affect its iron partitioning and Fe^{3+} content; it has been shown that the dissolution of Al^{3+} in bridgmanite at the top lower-mantle conditions can significantly enhance the Fe^{3+} occupancy in the A site of the lattice resulting in higher $K_D^{Bridg\text{-}fPer}$ (Irifune et al. 2010). The cause of these discrepancies may relate to dissimilar conditions under which the experiments were performed (great thermal gradients, pressure duration, chemical homogeneity, non-thermodynamic equilibrium, etc.) and /or in the compositions of starting materials, including different concentrations of Fe and Al used in the experiments.

The discovery of iron spin crossover in *fPer* led to the suggestion that $K_D^{Bridg\text{-}fPer}$ would behave differently in relevant high *P*-*T* conditions found in the deep lower mantle, decreasing from the mid-lower mantle to bottom lower mantle conditions, such that most of the iron partitions into *fPer* leaving *Bridg* essentially iron-free (Badro et al. 2003; Speziale et al. 2005). More recent theoretical and experimental studies on a pyrolite composition have found that $K_D^{Bridg\text{-}fPer}$ increases from approximately 0.5 at top-lower mantle conditions to 0.8-0.9, at about 800 km in depth due to the suggested coupled substitution of Al^{3+} and Fe^{3+} in *Bridg*, but then decreases to 0.4 or even lower due to the spin crossover of iron in *fPer* at mid-lower mantle conditions (Wood and Rubie 1996; Irifune et al. 2010; Vilella et al. 2015; Xu et al. 2016).

However, a high *P-T* diamond anvil cell study, using a pyrolite composition, has shown that $K_D^{\text{Bridg-fPer}}$ increases to 0.9 at bottom-lower mantle conditions, suggested to be due to the spin transition of Fe^{3+} in *Bridg* (Sinmyo and Hirose 2013). Recently, Fe-bearing bridgmanite has been reported to dissociate into Fe-rich phase, called H-Phase, and $MgSiO_3$-rich bridgmanite at deep lower mantle *P-T* conditions (Zhang et al. 2014), which can challenge the aforementioned conventional view of the iron index in the lower-mantle mineral assemblage. However, this report remains to be verified experimentally and theoretically. Thus far, a consensus on the iron partition coefficient across the spin transition in the lower-mantle assemblage has not yet been reached, especially under natural compositional, oxygen fugacity, and *P-T* environments.

Results

To date, a number of *Bridg*, *fPer* and other lower-mantle minerals have been identified as natural inclusions in diamonds, collected from Brazil, Canada, Guinea, Australia and some other countries, and subsequently analyzed (Kaminsky 2012 and references therein). The details of these finds and analytical procedures are presented elsewhere, including references to Tables 1 and 2 and Supplementary Table 1. Among them, are 19 *Bridg* + *fPer* pairs, each of which coexist in the same diamond, sometimes in a close ('touching') association, i.e., formed under equilibrium conditions. This relationship permits studies of the distribution and partitioning of iron and other elements within the media where those minerals originated within the lower mantle (Supplementary Table 1). We should note that the *Bridg* samples in these assemblages may have retrograde transformation into enstatite under ambient conditions, but a number of

physical and chemical characteristics established in previous studies justified their deep lower mantle origin as *Bridg* (e.g., Harte et al. 1999; Kaminsky 2012).

Ferropericlase

Ferropericlase in the lower-mantle compositional model has been typically assumed to exhibit a composition with *fe* = 0.08-0.11 and even more precisely, at c. 0.10 (Kesson and Fitz Gerald 1991). In the natural environment, however, *fPer* may be much more iron-rich, up to *fe* = 0.64, and sometimes even up to 0.90; as such, this does not correspond to the pyrolitic composition of the formation media. Recently, Fe-rich magnesiowüstite has been observed to occur in melting of subducted slabs in the mantle at approximately 300-700 km in depth (Thompson et al. 2016), providing a mechanism for the formation of very Fe-rich *fPer* in the lower mantle. TEM studies with the use of EDX and EEL spectroscopy demonstrated that ferric iron in *fPer* grains is located in exsolved non-stoichiometric Fe^{3+}-enriched clusters ($Mg_{1+x}Fe^{3+}_{2-x}O_{4-x/2}$), varying in size from 1–2 nm to 10–15 nm and comprising ~3.6 vol.% of *fPer*, while the remaining iron in *fPer* is in the ferrous, Fe^{2+} state (Fig. 2A) (Kaminsky et al. 2015a). Recent work by Nestola et al. (2016) demonstrated a possibility for studying the internal structure of ferropericlase and distribution of ferric iron in it (including its exsolved phases) with the use of *in situ* synchrotron Mössbauer spectroscopy. As the host diamond ascended through the uppermost lower mantle, these iron-rich clusters experience falling pressure conditions which resulted in their release and formation of 10-50 nm-sized magnesioferrite $MgFe^{3+}_2O_4$ crystals, developing along dislocations in *fPer* with a precise orientation relationship between both phases: $(022)_{mFer}$ // $(022)_{fPer}$; $(11\text{-}1)_{mFer}$ // $(11\ \text{-}1)_{fPer}$ and the zone axis for both phases is [2 -11] (Fig. 2B) (Kaminsky et al. 2015b).

Bridgmanite

Bridgmanite is a member of the perovskite family with an orthorhombic distortion of the ideal cubic perovskite structure and a general formula, $^{VIII/XII}A^{2+}\ ^{VI}B^{4+}O^{2-}_3$ (where VI, VIII and XII are cation fold positions), in which A larger (mainly divalent) pseudo-dodecahedral (eight/twelve-fold) site cations mostly include Mg, Fe^{2+}, Mn, Ni, Ca and some other elements, and B smaller six-fold site cations are Si, Al and partly Fe^{3+}. The analyzed natural lower-mantle bridgmanite samples have cation compositions as presented in Table 1.

Most of the grains have compositions close to stoichiometric *Bridg*. Some deficit in both cation groups is likely caused by the presence of other, non-analyzed cations, such as P and REE, which are characteristic for this group of minerals. Judging by crystal-chemical calculations (Table 1), all iron substitutes for Mg^{2+} in the A site and, most likely, is in the divalent form, Fe^{2+}, although McCammon et al. (1997), based on Mössbauer spectroscopy, suggested a significant portion of iron to be Fe^{3+}. There is no evidence for the presence of Fe^{3+} in the B site in natural *Bridg*. The three most Al-rich specimens (##BZ210; BZ241 and BZ242, all from Brazil) show excess in alumina in the amounts of 0.069-0.185. These amounts balance the deficit in cation site A of these specimens, implying the location of this portion of Al to be in the eight/twelve-fold pseudo-octahedral coordination position.

Partition coefficient of iron in natural bridgmanite – ferropericlase assemblages

The analysis of the iron index *fe* in co-existing *fPer* and *Bridg* grains and the partition

coefficient of iron $K_D^{Bridg\text{-}fPer}$ in all *Bridg* + *fPer* assemblages shows that two groups of assemblages can be distinguished (Table 2; Fig. 3A). The first group (Group A; 84 % of all pairs) forms an elongated cloud illustrating a general positive correlation between fe_{Bridg} = 0.032-0.138 and fe_{fPer} = 0.116-0.363. The correlation trend is close to trend Ia from the experimental data, confirming the regularity in Fe exchange between the two major lower-mantle minerals. The second group (Group B; 16 % of all grains) is composed of three specimens with almost constant fe_{fPer} = 0.173-0.193 and relatively high fe_{Bridg}, varying from 0.088 to 0.120; all specimens are high-Al varieties. This group lies outside of any experimental trends. The increase in *fe* of both natural *fPer* and *Bridg* from Group A is independent of the $K_D^{Bridg\text{-}fPer}$ values (0.169-0.479), while Group B, which has *fe* values in the same range as Group A, has elevated values of $K_D^{Bridg\text{-}fPer}$ = 0.433-0.657 (Fig. 3B).

Such variations in the iron indices and the bulk iron contents in the co-existing, major lower-mantle minerals differs drastically from what was expected for a pyrolytic lower mantle with a homogeneous distribution of iron in *fPer* and *Bridg* (Kesson and Fitz Gerald 1991; Wood 2000; Lee et al. 2004). According to the experimental and theoretical data for a bulk pyrolytic composition, where the total iron content in the system was fixed at *fe* = 0.09-0.15 (Irifune et al. 2010; Vilella et al. 2015; Xu et al. 2016), we should expect a decrease of the iron content in *Bridg* with an increase of the iron content in *fPer*. In reality, it is not the case, however, as both *fPer* and *Bridg* demonstrate the simultaneous, well-correlated increase of *fe* values (Figs. 3A-D).

Both groups of assemblages are characterized by similar concentrations of Ni in *fPer*, mainly corresponding to the bulk Ni contents in the mantle (6,052-11,212 ppm from Group A and 9,982-11,711 ppm from Group B) (Fig. 3C). However, one of the analyzed samples (#3-5 from Brazil) has a low concentration of Ni = 2437 ppm, and there are a number of low-Ni *fPer*

inclusions in diamond (Fig. 4A). Analysis of the Ni content in *fPer* as a function of the iron index shows that the *fPer* grains with *fe* of approximately 0.2 in deep-diamond inclusions (circled in Fig. 4B) have Ni contents close to the estimates of 8,000-12,000 ppm for the bulk pyrolytic composition; however, the Ni content drastically decreases with increasing iron index in *fPer,* especially for samples from Brazil (Fig. 3B). The samples with *fe* of more than 0.6 from Brazil have Ni contents less than 2000 ppm. So, the analyses of natural *fPer* grains show that the higher the iron index in the grain, the lower the Ni content.

There is a general (although not very strong) positive correlation between Ni and the partition coefficient of iron (Fig. 4A). The lowest $K_D^{\text{Bridg-fPer}}$ values (0.169 in sample # BZ120 and 0.204 in sample # 3-5) are characterized by the lowest Ni concentrations in *fPer*, whereas the samples with the highest $K_D^{\text{Bridg-fPer}}$ values (## BZ210, BZ241 and BZ242) are characterized with the highest Ni contents in *fPer*.

Discussion

Role of Ni and Al in the iron partition coefficient distribution

The Ni concentration in *fPer* indicates the presence of metallic iron phase(s) in the magmatic system of the deep mantle, as established by Frost et al. (2004). It was shown that the increasing weight fraction of metallic phase (suggesting the conditions present within the lowermost lower mantle) leads to a decrease of Ni concentration in the lower-mantle material and also to a decrease of the concentration of this element in coexisting *fPer* and *Bridg* (Ryabchikov and Kaminsky 2013). In this process, iron acts as a dilutant of Ni dissolved in

metal. According to experimental data (Frost et al. 2004; Frost and McCammon 2008), metal content in the lower mantle is estimated at 1 wt. % (10,000 ppm) before the release of metallic alloy. This implies that the *fPer* grains with high Ni concentrations were formed in media which did not contain metallic alloy (or its quantity was extremely small), suggesting these originated within the uppermost lower mantle, while the low Ni *fPer* grains were formed in the presence of metallic alloy within lower parts of the lower mantle. More than 40 % of the studied lower-mantle *fPer* grains are low-Ni and high-Fe inclusions. These variations in Fe and Ni concentrations in *fPer* point to a radial compositional gradient in the lower mantle at the time of the formation of these minerals, and the anti-correlation of Ni and Fe in *fPer* may be applied as a qualitative criterion of the depth of its origin.

The correlation between the $K_D^{Bridg\text{-}fPer}$ values and Ni concentrations in *fPer* (Fig. 4A) is not strong because of the presence of other elements in minerals, such as Al, Co, Mn, Na, et al. The major factor here is the Al impurity in *Bridg*, which is the real cause for the existence of the two groups of associations (Fig. 3D). Al_2O_3 in *Bridg* comprises 0.69-3.10 wt% in Group A and 10.04-12.58 wt% in Group B. In general, $K_D^{Bridg\text{-}fPer}$ correlates with the Al_2O_3 content in *Bridg*, which is particularly noticeable for the Brazilian samples (Fig. 5A). However, this correlation is quite weak (Fig. 5A,B) and requires further understanding.

The enrichment of *Bridg* with Al is strongly pressure dependent (Andrault et al. 2007). In the uppermost part of the lower mantle Al-rich phases, such as majorite and jeffbenite, still occur. In experiments at pressure conditions of 24-28 GPa these minerals dissociate, and the released Al is incorporated into *Bridg* (Irifune and Tsuchiya 2007). In the natural environment, the reverse scenario occurs: juvenile high-Al *Bridg* at 24-28 GPa releases Al with the formation

252 of Al-bearing phases, such as majorite and jeffbenite (formerly known as TAPP; Nestola et al.
253 2015).

254 As a result, the following scenario can be outlined for the lower mantle. *Bridg* has a high,
255 up to 10-12 wt% concentration of Al_2O_3, which is consistent with its bulk concentration in the
256 primitive mantle of 4-5 mol.% (e.g., McDonough and Sun 1995). Al occupies its position in both
257 cation sites, A and B. In each case Al substitutes for Si and divalent cations with oxygen-vacancy
258 formation as follows:

259 $$2\,^{VIII/XII}Al^{3+} + O^{2-} \rightarrow 2\,^{VIII/XII}(Mg,Fe)^{2+} + V^{0}\text{; and}$$

260 $$2\,^{VI}Al^{3+} + V^{0} \rightarrow 2\,^{VI}Si^{4+} + O^{2-}\text{ ;}$$

261 and in the case of Al positioning in both A and B sites, a charge-coupled mechanism, for which
262 no oxygen vacancies are required for charge balance, takes place (Richmond and Brodholt
263 1998):

264 $$^{VI}Al^{3+} + {}^{VIII/XII}Al^{3+} \rightarrow {}^{VI}Si^{4+} + {}^{VIII/XII}(Mg,Fe)^{2+}\text{;}$$

265 which, according to *ab initio* calculations, dominates at lower mantle pressures and temperatures
266 (Akber-Knutson and Bukowinski 2004). The concentration of Al in *Bridg,* particularly in the A
267 site may indicate the depth of the mineral's origin, because previous studies have shown that Al
268 concentration in *Bridg* increases with increasing pressure along a representative lower-mantle
269 geotherm (Irifune et al., 2010). Recently an experimental study of the system $MgSiO_3$-Al_2O_3
270 under pressures up to 52 GPa and 2000 K, with the use of sintered diamond anvils combined
271 with in situ synchrotron X-ray diffraction observations in a multi-anvil apparatus, demonstrated
272 that the Al_2O_3 content in bridgmanite increases from 12 mol.% at 27 GPa to 29 mol.% at 52 GPa,
273 suggesting that the Al_2O_3 content in bridgmanite can be used as a pressure indicator at pressures
274 above 30 GPa (Liu et al., 2016).

As was shown above (Section 2, Table 1), iron in *Bridg* is in the A site, most likely in a ferrous divalent form. *fPer* with depth (and correspondingly increasing pressure) has a decreasing concentration of Ni and increasing *fe* values, reflecting the increase in the iron content in the lower mantle. The decrease of Ni content in *fPer* may, therefore, be used as another qualitative geobarometer in the lower mantle.

In contrast to experimental conditions, most of which were performed with a pyrolitic compositions (*fe* = 0.05-0.15), our results on natural samples show that iron indices in *Bridg* and *fPer* have positive correlation (Fig. 3), demonstrating the total enrichments of the lower-mantle media in iron. This enrichment is correlated with the Ni (negatively, Fig. 3C) and Al_2O_3 (positively, Fig. 3D) concentrations, each of which is an independent criterion of the increasing pressure. One may conclude that the Fe content of the lower mantle increases with depth and may differ from the pyrolitic composition. Iron in *fPer* is predominantly in a divalent form; the share of Fe^{3+} ions is $Fe^{3+}/\Sigma Fe$ = 8-12 at% (Kaminsky et al. 2015a). Ferric iron in *fPer* grains is located in exsolved non-stoichiometric Fe^{3+}-enriched nanometer-sized clusters $Mg_{1+x}Fe^{3+}_{2-x}O_{4-x/2}$, while all remaining iron in *fPer* is in the ferrous, Fe^{2+}, state.

The discussion above opens new scenarios regarding the actual composition of the main minerals of the lower mantle, and the situation may be even more complex if we include additional phases which are present in the natural systems. Our interpretation of the new data on Fe, Ni and Al distribution in *Bridg* and *fPer* explains the controversies in aforementioned high *P-T* experimental results of experiments, carried out in simplified closed systems.

Regional differences in the distribution of iron in ferropericlase and bridgmanite

297 There are observed differences in the iron index of *fPer* values and related characteristics
298 from different regions. For example, *fPer* from Canada, South Australia and South Africa have *fe*
299 = 0.10-0.20 that are close to the pyrolite values. *fPer* from Guinea, along with similar *fe* values,
300 also has higher *fe* values of 0.25. Moreover, iron-rich *fPer* from Brazil (reaching the composition
301 of magnesiowüstite) comprises almost a half of all grains in this region (c. 46.5 %). It has been
302 suggested that such differences represent different depths, at which the host diamonds sampled
303 the lower mantle. In a pyrolytic lower mantle, the average amount of iron in the lower-mantle
304 minerals is commonly believed to be close to 10 %, chiefly distributed between *Bridg* and *fPer*
305 phases (Irifune et al. 2010). Here our analyses of the iron indices in these phases have shown that
306 the total iron content in some of these minerals can be much higher than what is expected for a
307 'normal' lower mantle. As shown in Fig. 2, the occurrence of these 'anomalous', high-Fe *fPer*
308 and high-Fe *Bridg* pairs with *fe* = 0.17-0.36 and 0.07-0.14, respectively, indicates that the lower
309 mantle is chemically inhomogeneous with respect to iron content at least in certain regions where
310 these assemblages originated.
311 Recent high-resolution seismic tomography studies have revealed detailed seismic
312 signatures of the lower mantle where strong seismic heterogeneities exist. Specifically, the Large
313 Low Shear Velocity Provinces (LLSVPs) beneath the central Pacific and South Africa, extending
314 from the core-mantle boundary up to approximately 1000 km above, exhibit reduced shear wave
315 velocities and enhanced densities (e.g., Garnero and McNamara 2008). These regions are
316 believed to contain dense, iron-rich piles that contribute to the 'low shear velocity' and high
317 density signatures in seismic observations; the iron enrichment in the regions may be due to
318 core-mantle interaction, residuals of the magma ocean, and/or recycling of primordial materials,
319 relative to the surrounding lower mantle (Garnero and McNamara 2008). On the other hand, thin

patches of the Ultralow Velocity Zones (ULVZs), that are 5 to 40 km thick patches directly above the core-mantle boundary, exhibit reduced *P*- and *S*-wave velocities by up to 10 % and 30 %, respectively, and enhanced densities of up to 10 % (Bower et al. 2011). These characteristics have been explained as a result of some partial melts and/or iron-enrichment in *Bridg* or silicate post-perovskite due to core-mantle reaction at the lowermost mantle (Garnero and McNamara 2008; Mao et al. 2010). We suggest that our analyzed *Bridg* + *fPer* pairs, which contain abnormally high iron indices, as shown in the second group in Fig. 3B,C,D, may originate from these regions that likely contain much higher amounts of iron than "normal" lower mantle regions.

Major differences in iron partitioning between natural samples and mineral physics results

In considering a natural system, we should expect the following scenario for depth, which should take into account the iron partitioning induced by the spin and valence transitions of iron ions proposed experimentally and theoretically, as well as significant iron chemistry heterogeneities at relevant P-T conditions of the lower mantle.

In the last decade, the discovery of a high-spin to low-spin crossover of Fe in the lower-mantle *fPer* and *Bridg* has been shown to influence their physical, chemical, rheological and transport properties that can produce significant geophysical and geochemical consequences for our understanding of the deep Earth (e.g., Badro et al. 2003; Cammarano et al. 2010; Lin et al. 2013; Wu and Wentzcovitch 2014; Yang et al. 2015). The spin crossover of Fe^{2+} in *fPer* has been theoretically predicted to occur and experimentally observed at *P*-*T* conditions corresponding to the middle and the lower parts of the lower mantle (e.g., Lin et al. 2007; Tsuchiya et al. 2006); though, the spin transition of Fe^{3+} in magnesioferrite and its associated effects remain unknown.

On the other hand, mineral physics studies of *Bridg* demonstrated that *Bridg* can contain a very significant amount of Fe^{3+} in its lattice at the top lower mantle conditions, in which both Fe^{2+} and Fe^{3+} in the pseudo-dodecahedral site (A site) of the orthorhombic structure likely remain in the high-spin state at lower-mantle pressures, while a high-spin to low-spin transition of Fe^{3+} in the octahedral site (B site) occurs at pressures of 15-50 GPa (e.g., Hsu et al. 2012; Lin et al. 2013). Recent theoretical calculations considering a wide range of oxygen fugacity conditions and different iron spin and valence states, in the lower-mantle pyrolite assemblage, have further indicated that the Fe^{3+} content in *Bridg* decreases with increasing depth in the lower mantle; at lowermost lower mantle conditions, Fe^{3+} content in *Bridg* becomes almost negligible (Xu et al. 2016). Analyses of the natural *Bridg* and *fPer* assemblages show that most of the iron residing in the A site of *Bridg* lattice is in the Fe^{2+} state, which confirms these mineral physics studies.

High *P-T* experiments have further shown that the partition coefficient $K_D^{\text{Bridg-fPer}}$ is observed to increase from approximately 0.5 at 23 GPa up to 0.85 at about 28 GPa (~800 km in depth) and that can be associated with the Al^{3+}-Fe^{3+} coupled substitution in *Bridg* in a pyrolytic composition, where iron ions partition almost equally between the *fPer* and *Bridg* lattices (Irifune et al. 2010). Results from such high P-T experiments showed that the $K_D^{\text{Bridg-fPer}}$ value stays almost constant at ~ 0.85 at pressures of between 28 and 40 GPa (~800-1000 km in depth) and then notably decreases to 0.4-0.5 with increasing pressures at 40-50 GPa (1000-1200 km in depth) (Irifune et al. 2010). This dramatic decrease is most likely associated with the spin transition of Fe^{2+} in *fPer*, which results in a volume collapse of about 2% (e.g., Lin et al. 2013) promoting iron ions in *Bridg* to favorably partition into the low-spin *fPer* which is energetically more stable than the high-spin *Bridg* and *fPer*. Without the alumina substitution in *Bridg* at such conditions, the $K_D^{\text{Bridg-fPer}}$ values decrease to approximately 0.2 (e.g., Sakai et al. 2009), i.e.,

366 lower than the value suggested from high *P-T* experiments using a pyrolytic composition (Irifune
367 et al. 2010). That is, in an alumina poor environment in the lower mantle, such as the olivine-rich
368 peridotite environment, the $K_D^{Bridg\text{-}fPer}$ value is expected to remain low at approximately 0.2 with
369 or without the spin transition effect. If the lower mantle is chemically pyrolytic, these changes in
370 the iron partitioning indicate that the deeper parts of the lower mantle, especially toward the
371 lowermost parts would likely contain iron-enriched, low-spin *fPer* and iron-poor, alumina-rich
372 *Bridg*, whereas in the upper parts of the lower mantle, especially at approximately 800 km in
373 depth, iron would almost equally partition between *Bridg* and *fPer* (Irifune et al. 2010).
374 Comparison of these experimental results with our analyses on natural samples, however, clearly
375 shows contradictory $K_D^{Bridg\text{-}fPer}$ values; the natural samples show very diverse $K_D^{Bridg\text{-}fPer}$ values
376 that cannot be simply explained by the alumina dissolution in *Bridg* and the spin transition of
377 Fe^{2+} in *fPer*. These major differences in the iron indices and $K_D^{Bridg\text{-}fPer}$ values demonstrate the
378 complex, inhomogeneous iron speciation and chemistry in the lower mantle that are well beyond
379 the knowledge of current mineral physics studies.
380

381 **Conclusions**

382

383 We conclude, based upon determined iron contents in coexisting natural *fPer* and *Bridg*
384 and on the distribution of the partition coefficient of iron in natural *Bridg* + *fPer* assemblages
385 that some areas in the deep lower mantle are iron-rich and differ markedly from a pyrolitic
386 composition, implying that the bulk composition of the Earth is non-chondritic.
387 The juvenile iron partitioning in the *Bridg* + *fPer* association ($K_D^{Bridg\text{-}fPer}$) is as low as 0.1-
388 0.2. During the crystallization of diamonds at relatively shallower depth of the lower mantle, in

389 which $K_D^{Bridg\text{-}fPer}$ increases to 0.4-0.5 and even as high as 0.7, they sample and deliver to the
390 surface such associations. This regularity, established on geological samples, was supported by
391 recently published theoretical calculations by Muir and Brodholt (2016), showing a decrease of
392 $K_D^{Brd\text{-}fPer}$ with depth from 0.32 to 0.06.

393 The details of the element partitioning between natural *Bridg* and *fPer*, in the lower mantle
394 (at least in some areas), are as follows:

395 • According to crystal-chemical calculations, iron in *Bridg* is ferrous, Fe^{2+}, in the A site,
396 substituting for Mg^{2+};

397 • Almost all iron in *fPer* is ferrous Fe^{2+}; the share of ferric, Fe^{3+}, iron in *fPer* is $Fe^{3+}/\Sigma Fe$
398 = 8-12 at%; Fe^{3+} is concentrated in exsolved clusters of $Mg_{1+x}Fe^{3+}_{2-x}O_{4-x/2}$, while all
399 remaining iron in *fPer* is in the ferrous, Fe^{2+}, state;

400 • Iron contents in both *Bridg* and *fPer* increase with depth (pressure), reflecting the
401 increasing Fe content in the lower part of the lower mantle;

402 • Al content in *Bridg* from the lower part of the lower mantle is at ~10-12 wt% Al_2O_3
403 (Table 2);

404 • Al in *Bridg* occurs mainly in the cation B site and partly in the cation A site, in both
405 cases substituting for Si, Mg and Fe with vacancy formation; and in the case of Al
406 positioning in both, B and A sites, a charge-balanced reaction.

407 These observations in natural samples cannot be simply explained by the dissolution of Al
408 in *Bridg* and the spin transition of Fe^{2+} in *fPer*. The differences between observations in natural
409 samples and experimental results should be taken into account in future calculations and
410 experimental works.

411

Acknowledgements

We thank Prof. W. Bassett and an anonymous reviewer for their careful, constructive reviews, which helped us to improve the manuscript. Particular thanks are also due to the Editor Fabrizio Nestola for his efficient handling of the manuscript.

References cited

Akber-Knutson, S., and Bukowinski, M.S.T. (2004) The energetics of aluminum solubility into $MgSiO_3$ perovskite at lower mantle conditions. Earth and Planetary Science Letters 220, 317– 330. DOI: 10.1016/S0012-821X(04)00065-2.

Andrault, D. (2001) Evaluation of (Mg,Fe) partitioning between silicate perovskite and magnesiowüstite up to 120 GPa and 2300 K. Journal of Geophysical Research 106 (B2). 2079-2087.

Andrault, D., Bolfan-Casanova, N., Bouhifd, M.A., Guignot, N., and Kawamoto, T. (2007) The role of Al-defects on the equation of state of Al–$(Mg,Fe)SiO_3$ perovskite. Earth and Planetary Science Letters 263, 167–179. DOI: 10.1016/j.epsl.2007.08.012.

Auzende, A.-L., Badro, J., Ryerson, F. J., Weber, P. K., Fallon, S. J., Addad, A., Siebert, J., and Fiquet, G. (2008) Element partitioning between magnesium silicate perovskite and ferropericlase: New insights into bulk lower-mantle geochemistry. Earth and Planetary Science Letters 269, 164-174. DOI: 10.1016/j.epsl.2008.02.001.

Badro, J., Fiquet, G., Guyot, F., Rueff, J.-P., Struzhkin, V.V., Vankó, G., and Monaco, G. (2003) Iron partitioning in Earth's mantle: Toward a deep lower mantle discontinuity. Science 300 (5620), 789-791. DOI: 10.1126/science.1081311.

Bower, D.J., Wicks, J.K., Gurnis, M., and Jackson, J.M. (2011) A geodynamic and mineral physics model of a solid-state ultralow-velocity zone. Earth and Planetary Science Letters 303, 193–202. DOI: 10.1016/j.epsl.2010.12.035.

Cammarano, F., Marquardt, H., Speziale, S., and Tackley, P.J. (2010) Role of iron-spin transition in ferropericlase on seismic interpretation: A broad thermochemical transition in the mid mantle? Geophysical Research Letters 37, L03308. DOI: 10.1029/2009GL041583.

Davies, R.M., Griffin, W.L., O'Reilly, S.Y., and Doyle, B.J. (2004) Mineral inclusions and geochemical characteristics of microdiamonds from the DO27, A154, A21, A418, DO18, DD17 and Ranch Lake kimberlites at Lac de Gras, Slave Craton, Canada. Lithos 77 (1-4), 39-55. DOI: 10.1016/j.lithos.2004.04.016

Dziewonski, A.M., and Anderson, D.L. (1981) Preliminary reference Earth model. Physics of the Earth and Planetary Interiors 25 (4), 297-356.

Frost, D.J., McCammon, C.A. (2008) The redox state of Earth's mantle. Annual Review of Earth and Planetary Sciences 36, 389-420. DOI: 10.1146/annurev.earth.36.031207.124322

Frost, D.J., Liebske, C., Langenhorst, F., McCammon, C. A., Trønnes, R.G., and Rubie D.C. (2004) Experimental evidence for the existence of iron-rich metal in the Earth's lower mantle. Nature 428, 409-412. DOI: 10.1038/nature02413.

Garnero, E., and McNamara, A. (2008) Structure and dynamics of Earth's lower mantle. Science, 320, 626-628. DOI: 10.1126/science.1148028.

Guyot, F., Madon, M., and Poirier, J.-P. (1988) X-ray microanalysis of high pressure/high temperature phases synthesized from natural olivine in the diamond–anvil cell. Earth and Planetary Science Letters 90, 52–64. DOI: 10.106/0012-821X(88)90110-0.

Harte, B., Harris, J.W., Hutchison, M.T., Watt, G.R., and Wilding, M.C. (1999) Lower mantle mineral associations in diamonds from Sao Luiz, Brazil. Geochemical Society Special Publication No. 6, 125- 153.

Hayman, P.C., Kopylova, M.G., and Kaminsky, F.V. (2005) Lower mantle diamonds from Rio Soriso (Juina, Brazil). Contributions to Mineralogy and Petrology 149 (4), 430-445. DOI: 10.1007/s00410-005-0657-8.

Hsu, H., Yu, Y.G., and Wentzcovitch, R.M. (2012) Spin crossover of iron in aluminous $MgSiO_3$ perovskite and post-perovskite. Earth and Planetary Science Letters 294, 19-26. DOI: 10.1016/j.epsl.2010.02.031.

Hutchison, M.T. (1997) Constitution of the deep transition zone and lower mantle shown by diamonds and their inclusions. Unpublished PhD Thesis. University of Edinburgh, UK. Vol.1, 340 pp., Vol. 2 (Tables and Appendices), 306 pp.

Irifune, T. (1994) Absence of an aluminous phase in the upper part of the Earth's lower mantle. Nature 370, 131-133. DOI: 10.1038/370131a0.

Irifune, T., and Tsuchiya, T. (2007) Mineralogy of the Earth – Phase transitions and mineralogy of the lower mantle. Treatise on Geophysics, vol. 2, pp. 33-62.

Irifune T., Shinmei T., McCammon C.A., Miyajima N., Rubie D.C., and Frost D.J. (2010) Iron partitioning and density changes of pyrolite in Earth's lower mantle. Science 327(5962), 193-195. DOI: 10.1126/science.1181443

Kaminsky, F.V. (2012) Mineralogy of the lower mantle: A review of 'super-deep' mineral inclusions in diamond. Earth-Science Reviews 110 (1-4), 127-147. DOI: 10.1016/j.earscirev.2011.10.005.

Kaminsky, F.V., Ryabchikov, I.D., McCammon, C., Longo, M., Abakumov, A.M., Turner, S., and Heidari, H. (2015a) Oxidation potential in the Earth's lower mantle as recorded from ferropericlase inclusions in diamond. Earth and Planetary Science Letters 417, 49-56. DOI: 10.1016/j.epsl.2015.02.029.

Kaminsky, F.V., Wirth, R., and Schreiber, A. (2015b) A microinclusion of lower-mantle rock and some other lower-mantle inclusions in diamond. Canadian Mineralogist 53 (1), 83-104. DOI: 10.3749/canmin.1400070.

Katsura, T., and Ito, E. (1996) Determination of Fe–Mg partitioning between perovskite and magnesiowüstite. Geophysical Research Letters 23 (16), 2005–2008.

Kennett, B., Engdahl, E., and Buland, R. (1995) Constraints on seismic velocities in the Earth from traveltimes. Geophysical Journal International 122 (1), 108-124. DOI: 10.1111/j.1365-246X.1995.tb03540.x.

Kesson, S.E., and Fitz Gerald, J.D. (1991) Partitioning of MgO, FeO, NiO, MnO and Cr_2O_3 between magnesian silicate perovskite and magnesiowüstite: implications for the origin of inclusions in diamond and the composition of the lower mantle. Earth and Planetary Science Letters 111 (2-4), 229–240.

Kesson S.E., Fitz Gerald, J.D., and Shelley, J.M. (1998) Mineralogy and dynamics of a pyrolite lower mantle. Nature 393 (6682) (252-255. DOI : 10.1016/0012-821X(92)90181-T.

Kesson, S.E., Fitz Gerald, J.D., O'Neill, H.St.C., and Shelley, J.M.G. (2002) Partitioning of iron between magnesian silicate perovskite and magnesiowüstite at about 1 Mbar. Physics of the Earth and Planetary Interiors 131, 295–310. DOI : 10.1016/S0031-9201(02)00063-8.

Kobayashi, Y., Kondo, T., Ohtani, E., Hirao, N., Miyajima, N., Yagi, T., Nagase, T., and Kikegawa, T. (2005) Fe–Mg partitioning between (Mg, Fe)SiO_3 post-perovskite, perovskite, and magnesiowüstite in the Earth's lower mantle. Geophysical Research Letters 32, L19301. DOI: 10.1029/2005GL023257.

Lee, K.K.M., O'Neill, B., Panero, W.R., Shim, S.H., Benedetti, L.R., and Jeanloz, R. (2004) Equations of state of the high-pressure phases of a natural peridotite and implications for the Earth's lower mantle. Earth and Planetary Science Letters 223 (3-4), 381– 393. DOI: 10.1016/j.epsl.2004.04.033.

Lin, J.F., Vankó, G., Jacobsen, S.D., Iota, V., Struzhkin, V.V., Prakapenka, V.B., Kuznetsov, A., and Yoo, C.-S. (2007) Spin transition zone in Earth's lower mantle. Science, 317, 1740-1743. DOI: 10.1126/science.1144997.

Lin, J-F., Speciale, S., Mao, Z., and Marquardt, H. (2013) Effects of the electronic spin transitions of iron in lower mantle minerals: implications for deep mantle geophysics and geochemistry. Reviews in Geophysics 51 (2), 244-275. DOI: 8755-1209/13/10.1002/rog.20010.

Liu, Z., Irifune, T., Nishi, M., Tange, Y., Arimoto, T., and Shinmei, T. (2016) Phase relations in the system $MgSiO_3$–Al_2O_3 up to 52 GPa and 2000 K. Physics of the Earth and Planetary Interiors 257, 18–27. 10.1016/j.pepi.2016.05.006.

Mao, Z., Lin, J.F., Jacobs, C., Watson, H., Xiao,Y., Chow, P., Alp, E.E., and Prakapenka, V.B. (2010) Electronic spin and valence states of Fe in $CaIrO_3$-type post-perovskite in the Earth's lowermost mantle. Geophysical Research Letters 37, L22304.

McCammon, C., Hutchison, M.T., and Harris J.W. (1997) Ferric iron content of mineral inclusions in diamonds from São Luiz: A view into the lower mantle. Science 278 (5337), 434-436. DOI: 10.1126/science.278.5337.434

McDonough, W.F., and Sun, S.-S. (1995) The composition of the Earth. Chemical Geology 120, 223– 253. DOI: 10.1016/0009-2541(94)00140-4.

Muir, J.M.R., and Brodholt, J.P. (2016) Ferrous iron partitioning in the lower mantle. Physics of the Earth and Planetary Interiors 257, 12–17. DOI: 1 0.1016/j.pepi.2016.05.008.

Murakami, M., Hirose, K., Sata, N., and Ohishi, Y. (2005) Post-perovskite phase transition and mineral chemistry in the pyrolitic lowermost mantle. Geophysical Research Letters 32, L03304. DOI: 10.1029/2004GL021956.

Nestola, F., Burnham, A., Peruzzo, L., Tauro, L., Alvaro, M., Walter, M.J., and Gunther, M. (2015) Jeffbenite, IMA 2014-097. CNMNC Newsletter No. 24, April 2015, page 250. Mineralogical Magazine 79, 247-251. DOI: 10.1180/minmag.2016.080.059.

Nestola, F., Cerantola, V., Milani, S., Anzolini, C., McCammon, C., Novella, D., Kupenko, I., Chumakov, A., Rüffer, R., and Harris, J.W. (2016) Synchrotron Mössbauer Source technique for in situ measurement of iron-bearing inclusions in natural diamonds. Lithos, on-line. DOI: 10.1016/j.lithos.2016.06.016.

Richmond, N.C., and Brodholt, J.P. (1998. Calculated role of aluminum in the incorporation of ferric iron into magnesium silicate perovskite. American Mineralogist 83 (9-10), 947-951.

Ryabchikov, I.D., and Kaminsky, F.V. (2013) Oxygen potential of diamond formation in the lower mantle. Geology of Ore Deposits 55 (1), 1-12. DOI: 10.1134/S1075701513010066.

Sakai, T., Ohtani, E., Terasaki, H., Sawada, N., Kobayashi, Y., Miyahara, M., Nishijima, M., Hirao, N., Ohishi, Y., and Kikegawa, T. (2009. Fe–Mg partitioning between perovskite and

546 ferropericlase in the lower mantle. American Mineralogist 94, 921–925. DOI:
547 10.2138/am.2009.3123.
548 Sinmyo, R., and Hirose, K. (2013) Iron partitioning in pyrolitic lower mantle. Physics and
549 Chemistry of Minerals 40, 107–113. DOI: 10.1007/s00269-012-0551-7.
550 Speziale, S., Milner, A., Lee, V.E., Clark, S.M., Pasternak, M.P., and Jeanloz, R. (2005) Iron
551 spin transition in Earth's mantle. Proceedings of the National Academy of Sciences of the
552 U.S.A. 102, 17918–17922. DOI: 10.1073/pnas.0508919102.
553 Stachel, T., Harris, J.W., Brey, G.P., and Joswig, W. (2000) Kankan diamonds (Guinea) II: lower
554 mantle inclusion parageneses. Contributions to Mineralogy and Petrology 140 (1), 16-27.
555 DOI: 10.1007/s004100000174.
556 Tange, Y., Takahashi, E., Nishihara, Y., Funakoshi, K., and Sata, N (2009) Phase relations in the
557 system MgO-FeO-SiO_2 to 50 GPa and 2000° C: An application of experimental techniques
558 using multianvil apparatus with sintered diamond anvils. Journal of Geophysical Research
559 114, B02,214.
560 Tappert, R., Foden, J., Stachel, T., Muehlenbachs, K., Tappert, M., and Wills, K. (2009) Deep
561 mantle diamonds from South Australia: A record of Pacific subduction at the Gondwanan
562 margin. Geology 37 (1), 43–46. DOI: 10.1130/G25055A.1.
563 Thomson, A.R., Walter, M.J., Kohn, S.C., and Brooker, R.A. (2016) Slab melting as a barrier to
564 deep carbon subduction. Nature 529, 76-79.
565 Tsuchiya, T., Wentzcovitch, R.M., da Silva, C.R.S., and de Gironcoli, S. (2006) Spin transition
566 in magnesiowüstite in Earth's lower mantle. Physical Review Letters 96, 198501. DOI:
567 10.1103/PhysRevLett.96.198501

568 Vilella, K., Shim, S.-H., Farnetani, C.G., and Badro, J. (2015) Spin state transition and
569 partitioning of iron: Effects on mantle dynamics. Earth and Planetary Science Letters 417,
570 57–66. DOI:10.1016/j.epsl.2015.02.009.
571 Wood, B.J. (2000) Phase transformations and partitioning relations in peridotite under lower
572 mantle conditions. Earth and Planetary Science Letters 174 (3-4), 341-354.
573 Wood, B. J., and Rubie, D. C. (1996) The effect of alumina on phase transformations at the 660-
574 kilometer discontinuity from Fe-Mg partitioning experiments. Science 273, 1522-1524.
575 Wu, Z., and Wentzcovitch, R.M. (2014) Spin crossover in ferropericlase and velocity
576 heterogeneities in the lower mantle. Proceedings of the National Academy of Sciences of
577 the United States of America 111, 10468-10472. DOI: 10.1073/pnas.1322427111.
578 Xu, S., Lin, J.-F., and Morgan, D. (2016) Iron Speciation Induced Chemical and Seismic
579 Heterogeneities in the Lower Mantle. Proceedings of the National Academy of Sciences of
580 the U.S.A. (submitted).
581 Yang, J., Tong, X., Lin, J.F., Tomioka, N., Okuchi, T., and Prakapenka, V.B. (2015) Elasticity of
582 Ferropericlase across the Spin Crossover in the Earth's Lower Mantle. Scientific Reports 5,
583 17188. DOI: 10.1038/srep17188.
584 Zhang, L., Meng, Y., Yang, W., Wang, L., Mao, W.L., Zeng, Q.S., Jeong, J.S., Wagner, A.J.,
585 Mkhoyan, K.A., Liu, W., Xu, R., and Mao, H.K. (2014) Disproportionation of
586 $(Mg,Fe)SiO_3$ perovskite in Earth's deep lower mantle. Science 344, 879-882.
587 Zedgenizov D.A., Kagi H., Shatsky V.S., and Ragozin A.L. (2014) Local variations of carbon
588 isotope composition in diamonds from Sao-Luis (Brazil): evidence for heterogenous carbon
589 reservoir in sublithospheric mantle. Chemical Geology 240 (1-2), 114-124. DOI:
590 10.1016/j.chemgeo.2013.10.033.

Tables

Table 1. Cation fractions of natural lower-mantle bridgmanite (in atomic numbers). A_{total} and B_{total} represent the total cation fraction in the A and B site, respectively.

Note: *References: 1 – Hutchison (1997), 2 – Zedgenizov et al. (2014), 3 – Hayman et al. (2005), 4 - Davies et al. (2004), 5 – Stachel et al. (2000), 6 – Tappert et al. (2009).

Table 2. Compositions of coexisting bridgmanite and ferropericlase included in lower-mantle diamonds.

Note: * Bridg: bridgmanite; fPer: ferropericlase; Di?: suggested diopside; CaSiPrv: CaSi-perovskite; 'Ol': phase with an olivine composition; SiMg: unidentified Si-Mg phase; Ni: native Ni; Ga: garnet.

** Reference numbers are the same as in Table 1.

Captions to figures

Figure 1. Summary of literature experimental results of iron partitioning between bridgmanite and ferropericlase at high pressures and temperatures. A – fe_{Bridg} vs. fe_{fPer} in all experiments performed to date. I and II – general trends. B – partition coefficient fe_{fPer} under different pressure values.

614

615 **Figure 2**. Exsolution of Fe^{3+}-rich phases in ferropericlase. A - $Mg_{1.30}Fe^{3+}_{1.80}O_4$ truncated
616 octahedra (bright) in a ferropericlase dark matrix; high-angle annular dark field scanning
617 transmission electron-microscopy image by A. Abakumov (Kaminsky et al. 2015a). B –
618 Magnesioferrite, $MgFe^{3+}_2O_4$, octahedral and cubic grains, developed along dislocations in
619 ferropericlase. Dark field TEM image by R. Wirth (Kaminsky et al. 2015b).

620

621 **Figure 3**. Iron indices *fe* = $Fe/(Fe+Mg)_{at}$ in coexisting natural ferropericlase and bridgmanite in
622 lower-mantle diamond inclusions. A – General plot. B – With $K_D^{Bridg\text{-}fPer}$ values, shown as
623 circles, the radii of which are proportional to the $K_D^{Bridg\text{-}fPer}$ values. C – With Ni concentrations in
624 ferropericlase, shown as circles, the radii of which are proportional to the Ni concentrations. D –
625 With Al_2O_3 concentrations in bridgmanite, shown as circles, the radii of which are proportional
626 to the Al_2O_3 concentrations. Four groups of samples from Brazil, Canada, Guinea, and Australia
627 with the *fPer* and *Bridg* grains that associate with each other are used.

628

629 **Figure 4**. Variations of Ni concentrations in natural ferropericlase. A - $K_D^{Bridg\text{-}fPer}$ vs. Ni content
630 in ferropericlase. B - Ni content vs. iron index in all analyzed to date ferropericlase grains
631 entrapped by lower-mantle diamonds. Data from Kaminsky et al. (2012) and references therein.

632

633 **Figure 5**. Iron partitioning coefficient $K_D^{Bridg\text{-}fPer}$ vs. Al_2O_3 content in bridgmanite. A – General
634 plot. B – With Ni concentrations in ferropericlase from Brazil, Canada, Guinea and Australia,
635 shown as circles, the radii of which are proportional to the Ni contents.

636

637

638 **Supporting information**

639

640 **Table S1**. Chemical compositions of coexisting natural bridgmanite and ferropericlase grains

641 included in diamond.

This is a preprint, the final version is subject to change, of the American Mineralogist (MSA)
Cite as Authors (Year) Title. American Mineralogist, in press.
(DOI will not work until issue is live.) DOI: http://dx.doi.org/10.2138/am-2017-5949

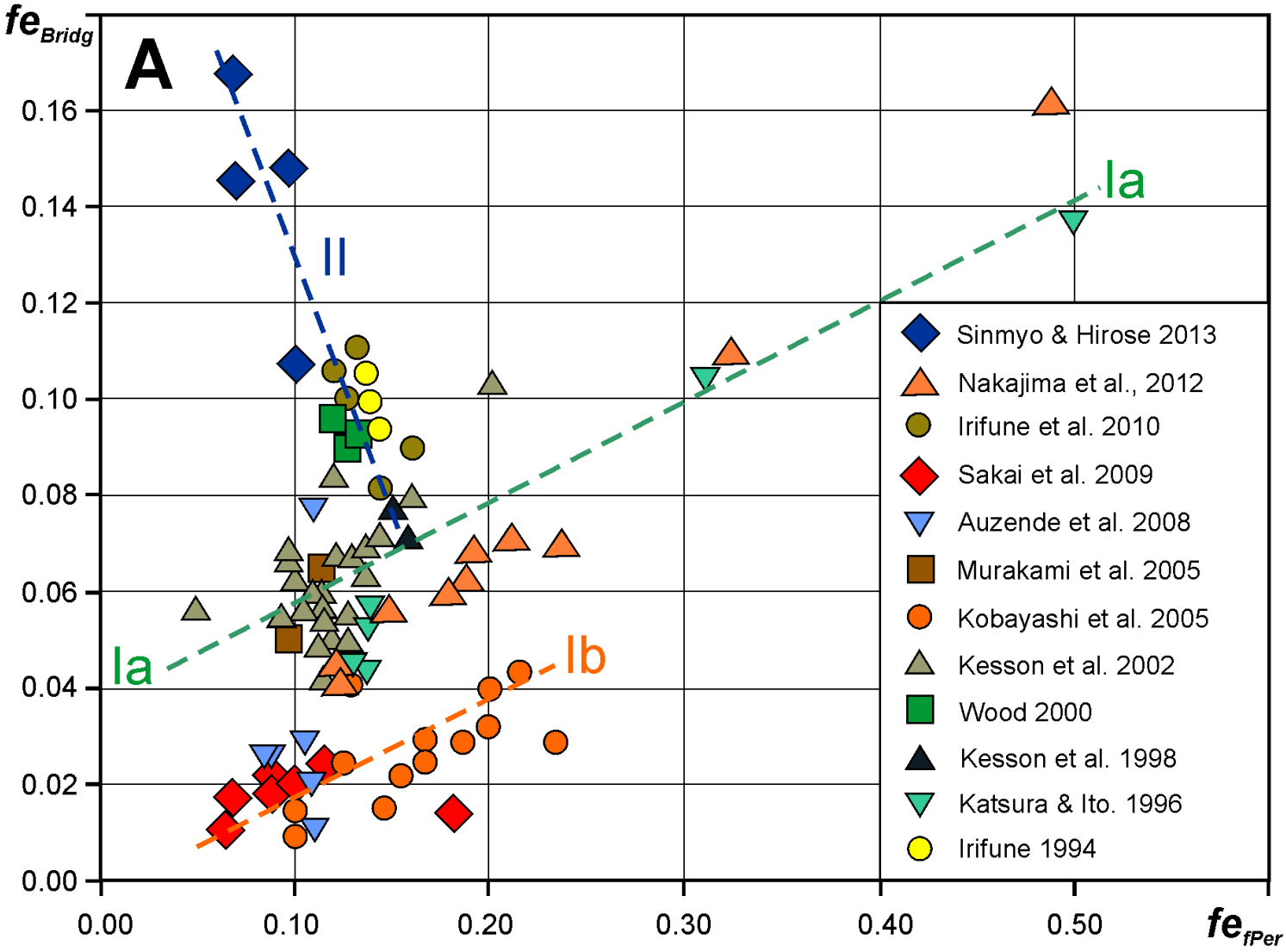

Figure 1A

This is a preprint, the final version is subject to change, of the American Mineralogist (MSA)
Cite as Authors (Year) Title. American Mineralogist, in press.
(DOI will not work until issue is live.) DOI: http://dx.doi.org/10.2138/am-2017-5949

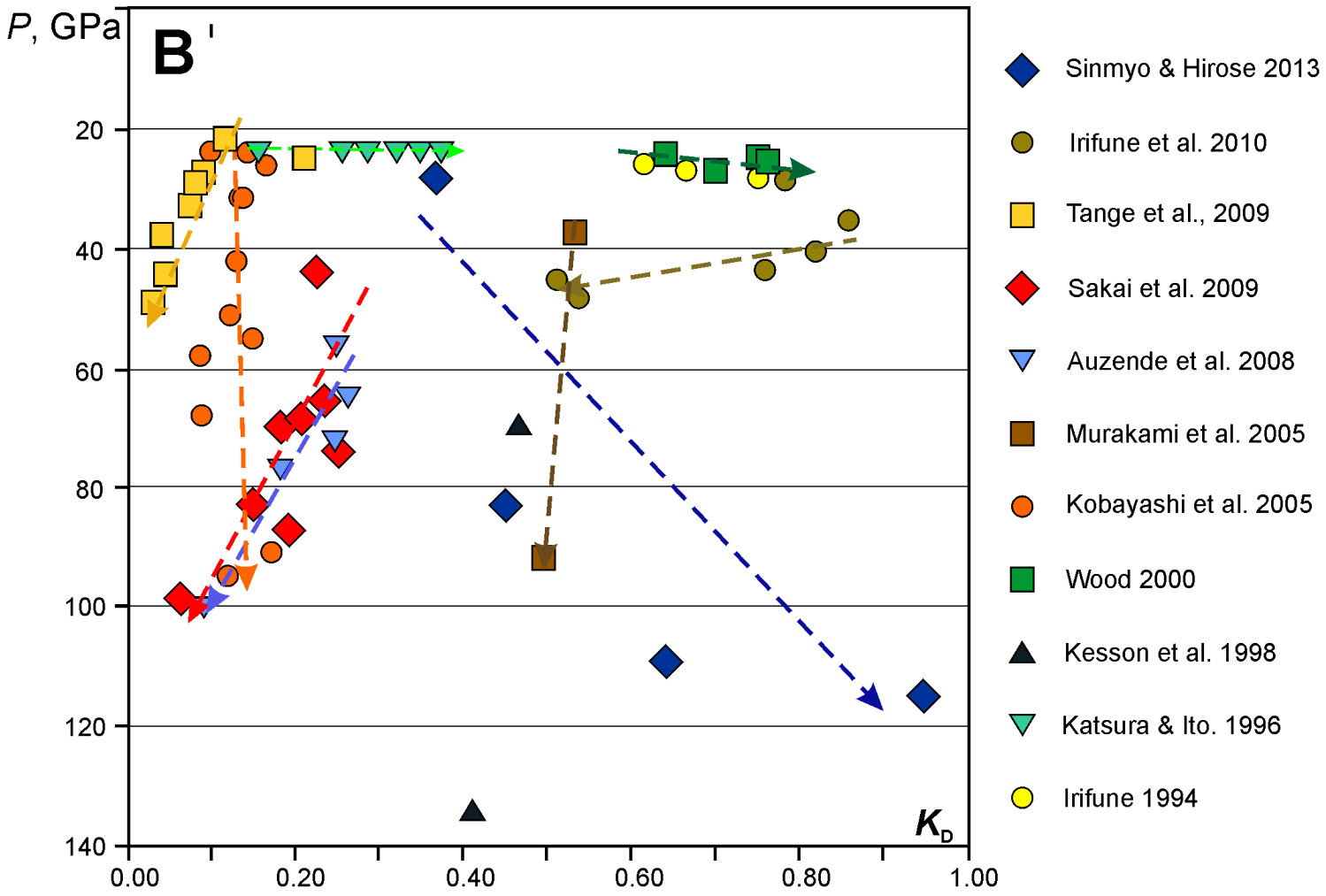

Figure 1B

This is a preprint, the final version is subject to change, of the American Mineralogist (MSA)
Cite as Authors (Year) Title. American Mineralogist, in press.
(DOI will not work until issue is live.) DOI: http://dx.doi.org/10.2138/am-2017-5949

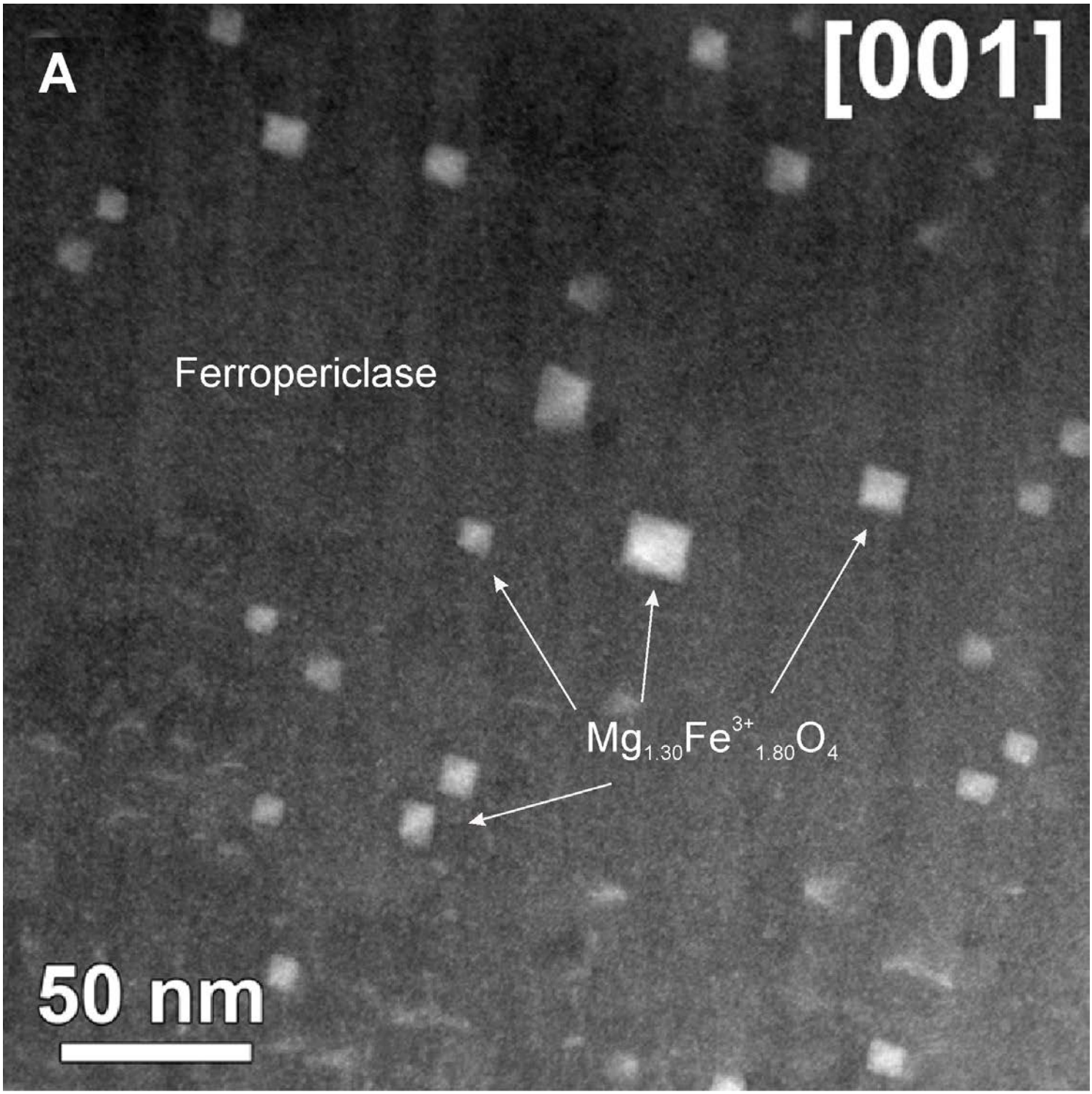

Figure 2A

This is a preprint, the final version is subject to change, of the American Mineralogist (MSA)
Cite as Authors (Year) Title. American Mineralogist, in press.
(DOI will not work until issue is live.) DOI: http://dx.doi.org/10.2138/am-2017-5949

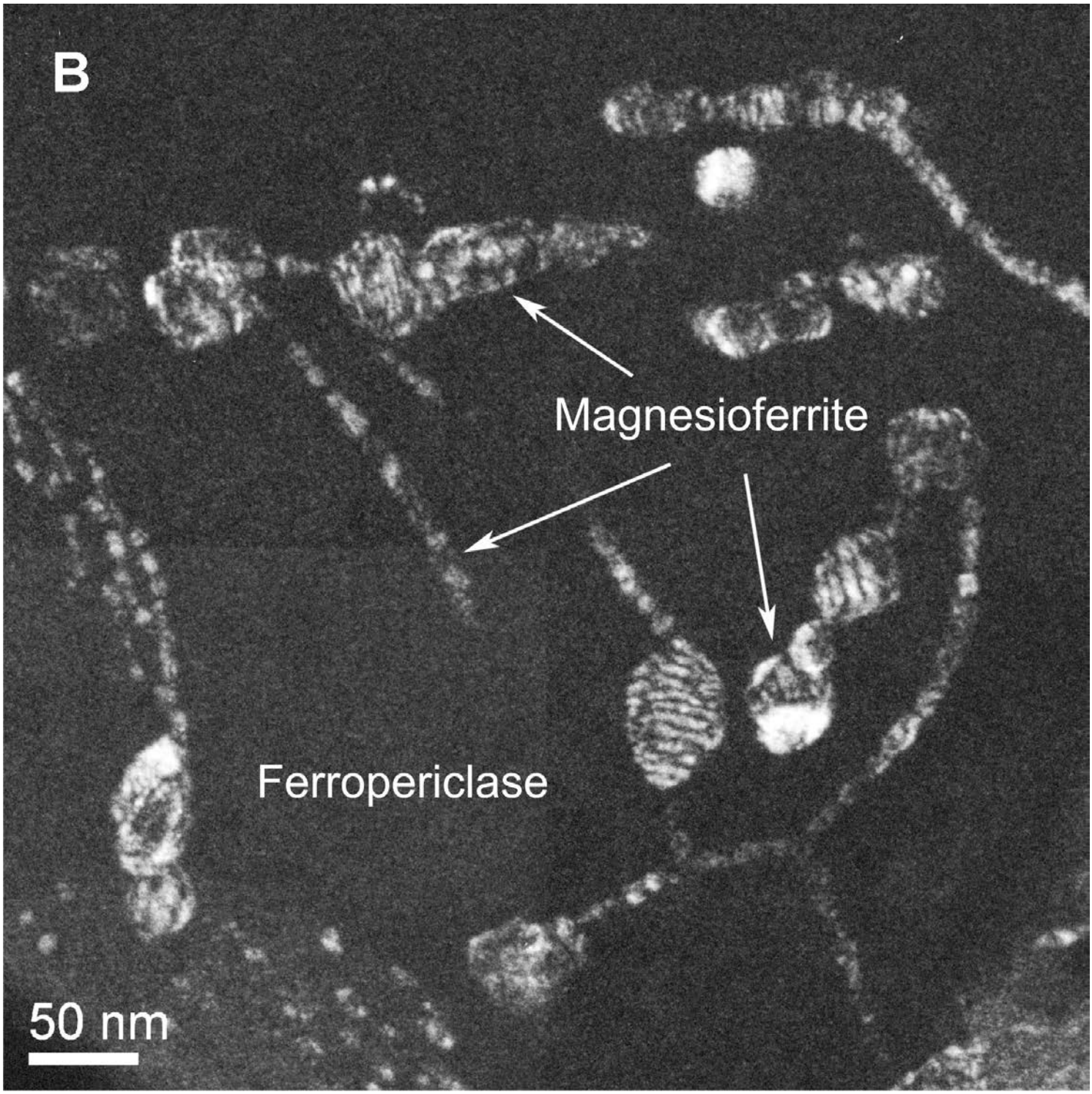

Figure 2B

This is a preprint, the final version is subject to change, of the American Mineralogist (MSA)
Cite as Authors (Year) Title. American Mineralogist, in press.
(DOI will not work until issue is live.) DOI: http://dx.doi.org/10.2138/am-2017-5949

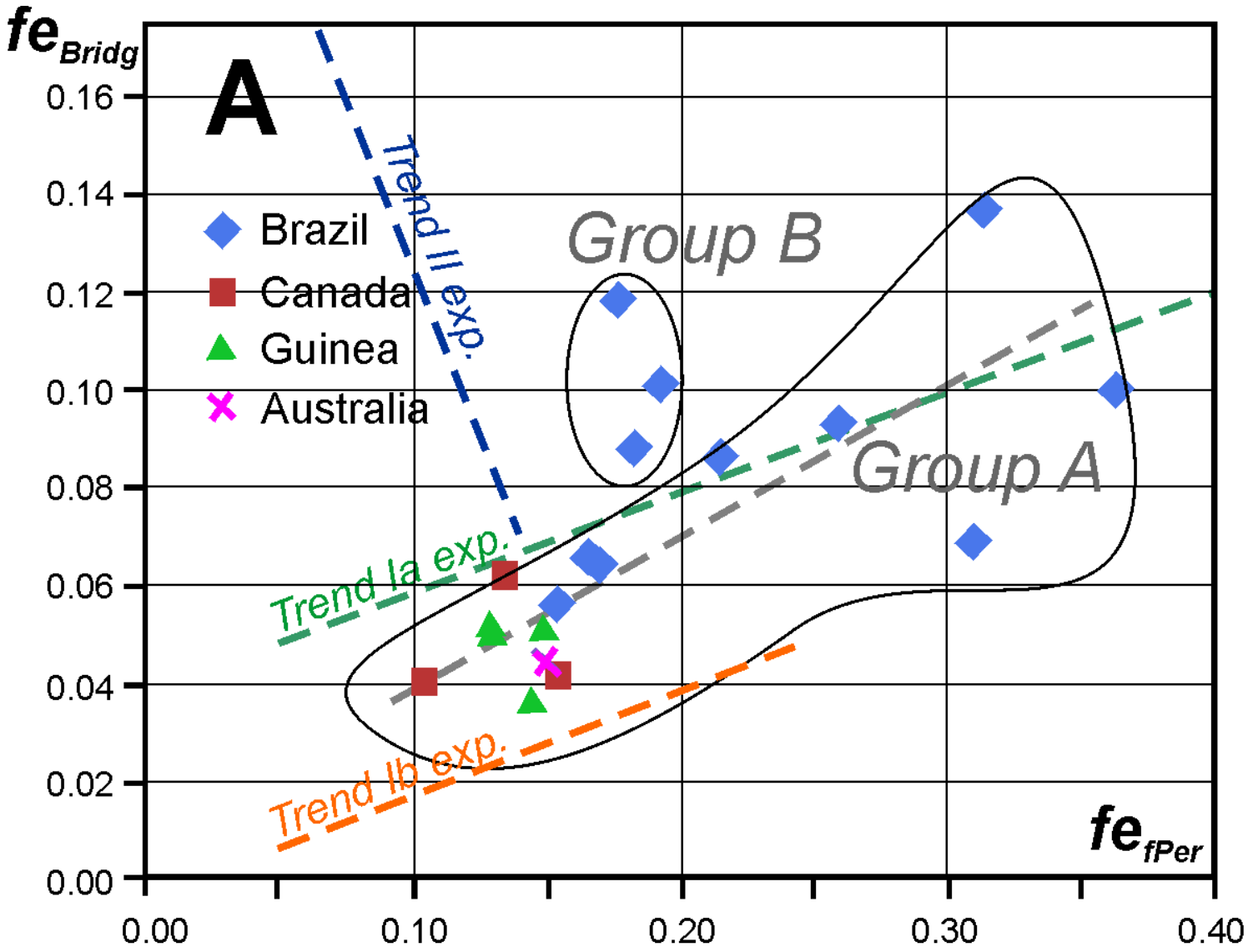

Figure 3A

This is a preprint, the final version is subject to change, of the American Mineralogist (MSA)
Cite as Authors (Year) Title. American Mineralogist, in press.
(DOI will not work until issue is live.) DOI: http://dx.doi.org/10.2138/am-2017-5949

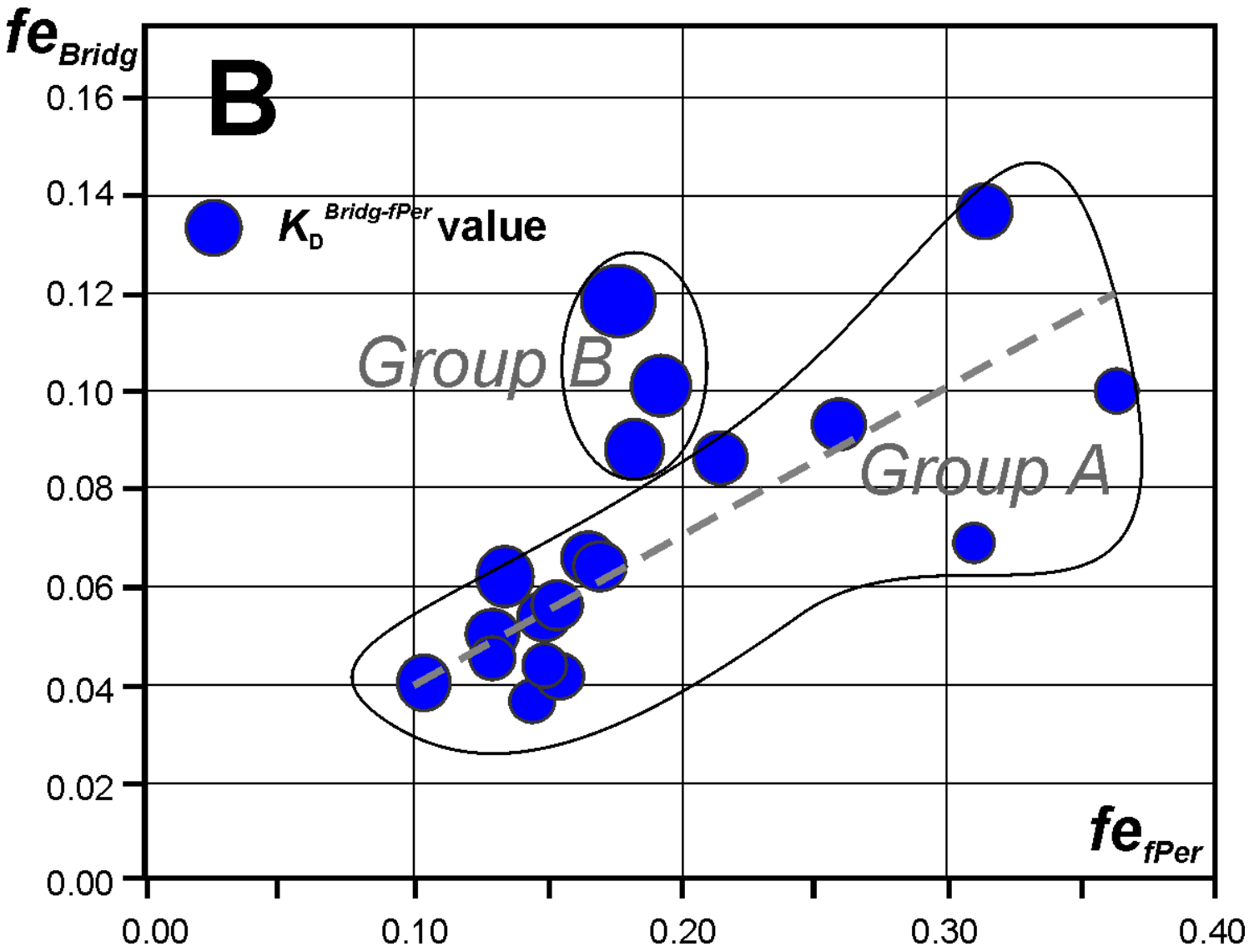

Figure 3B

This is a preprint, the final version is subject to change, of the American Mineralogist (MSA)
Cite as Authors (Year) Title. American Mineralogist, in press.
(DOI will not work until issue is live.) DOI: http://dx.doi.org/10.2138/am-2017-5949

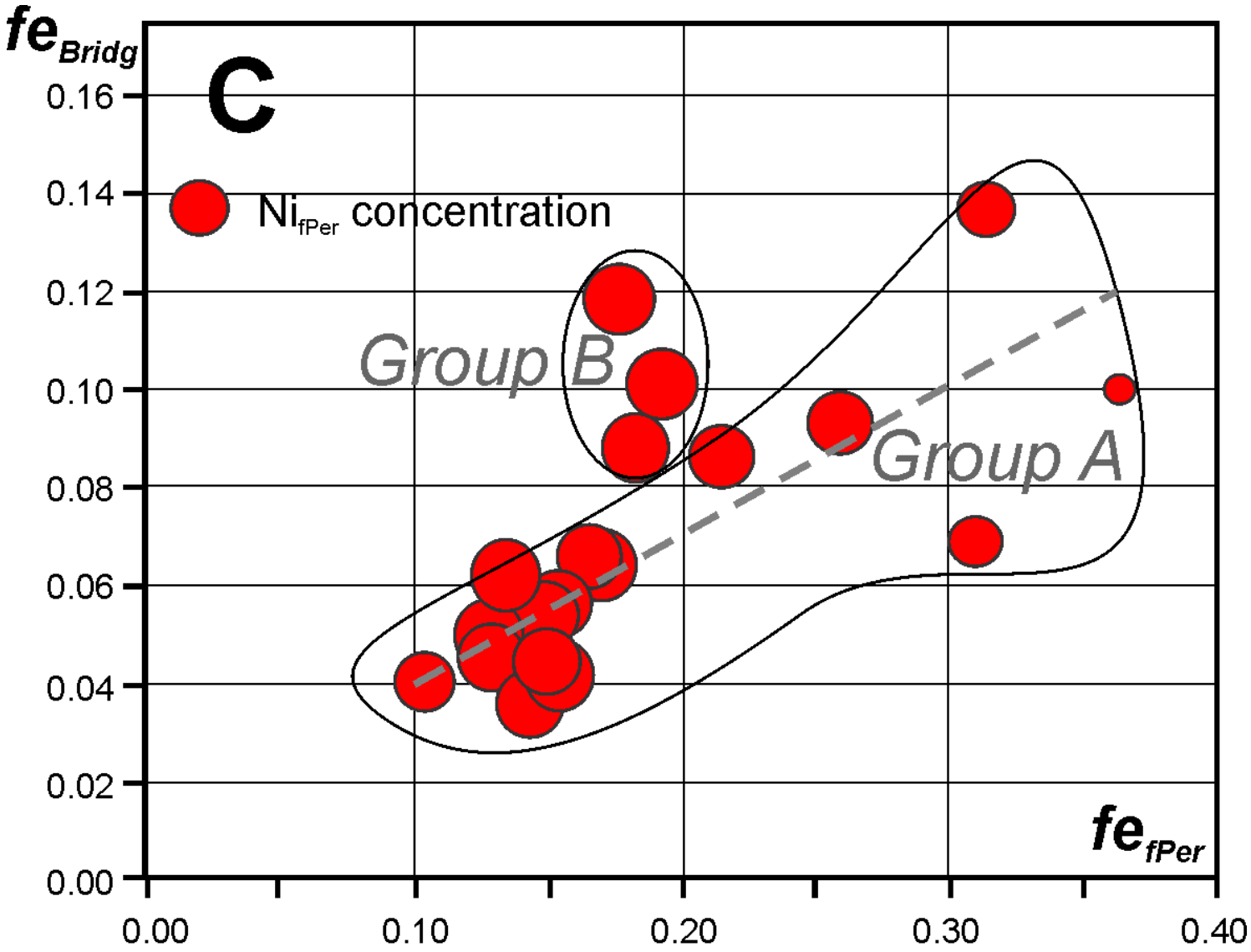

Figure 3C

This is a preprint, the final version is subject to change, of the American Mineralogist (MSA)
Cite as Authors (Year) Title. American Mineralogist, in press.
(DOI will not work until issue is live.) DOI: http://dx.doi.org/10.2138/am-2017-5949

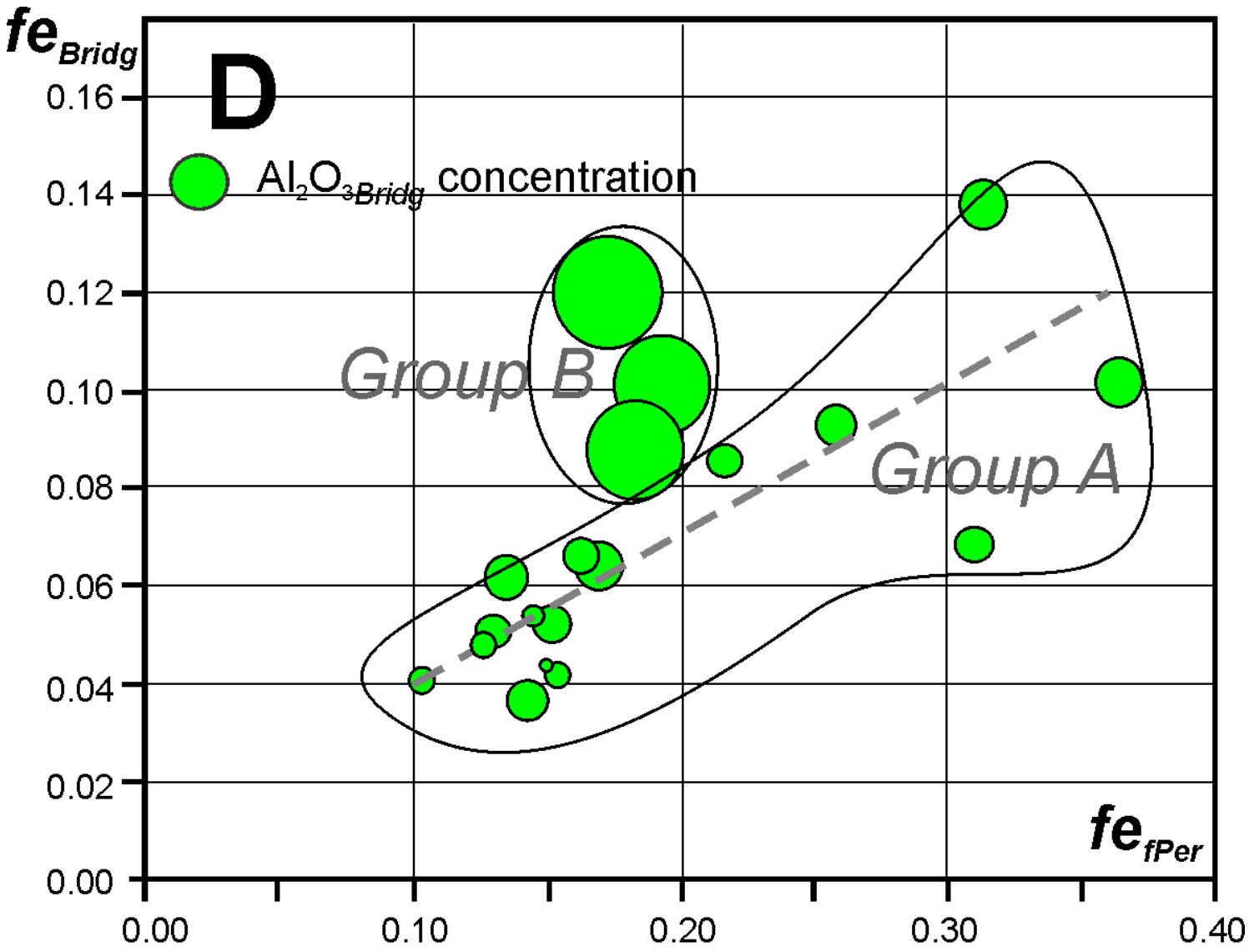

Figure 3D

This is a preprint, the final version is subject to change, of the American Mineralogist (MSA)
Cite as Authors (Year) Title. American Mineralogist, in press.
(DOI will not work until issue is live.) DOI: http://dx.doi.org/10.2138/am-2017-5949

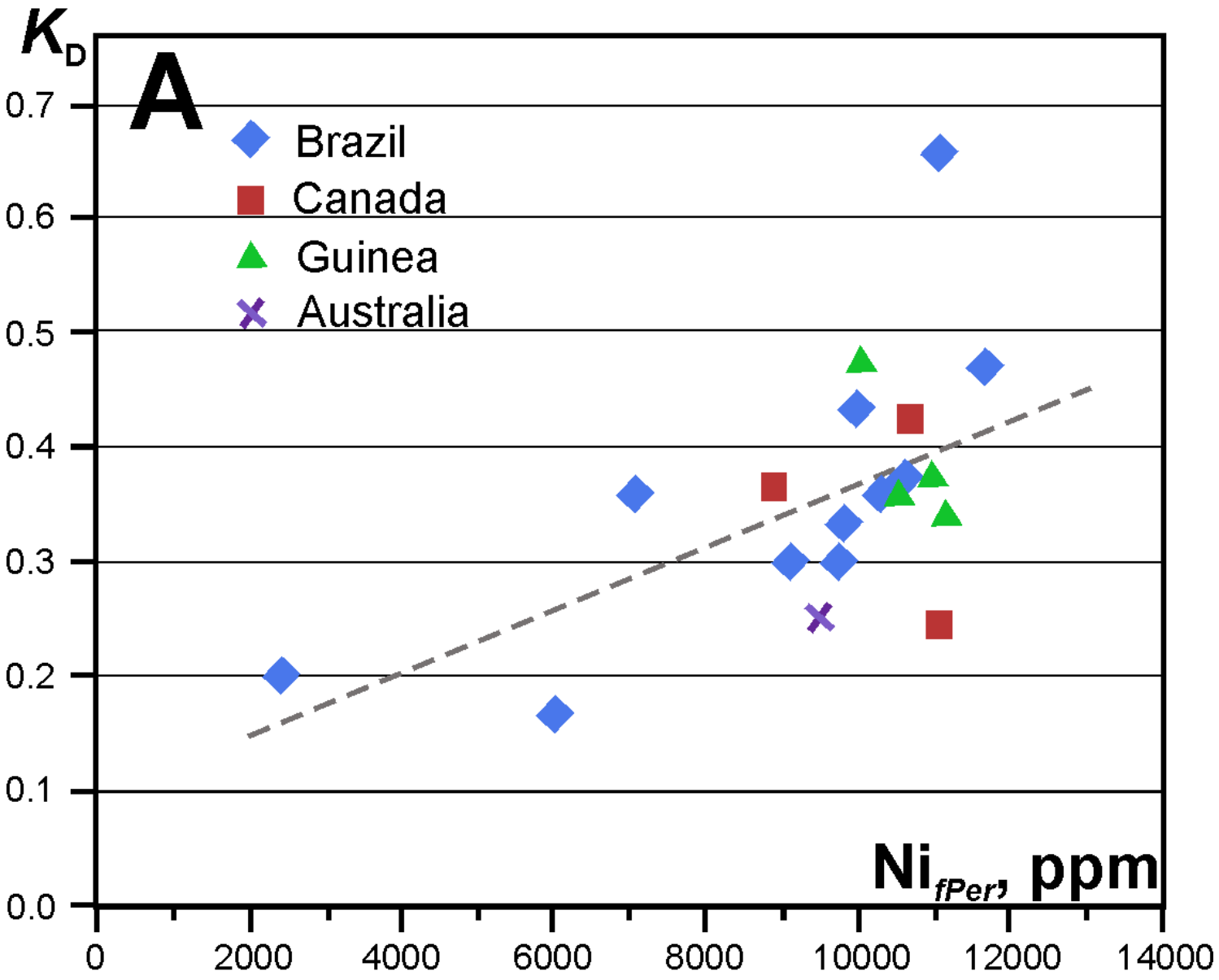

Figure 4A

This is a preprint, the final version is subject to change, of the American Mineralogist (MSA)
Cite as Authors (Year) Title. American Mineralogist, in press.
(DOI will not work until issue is live.) DOI: http://dx.doi.org/10.2138/am-2017-5949

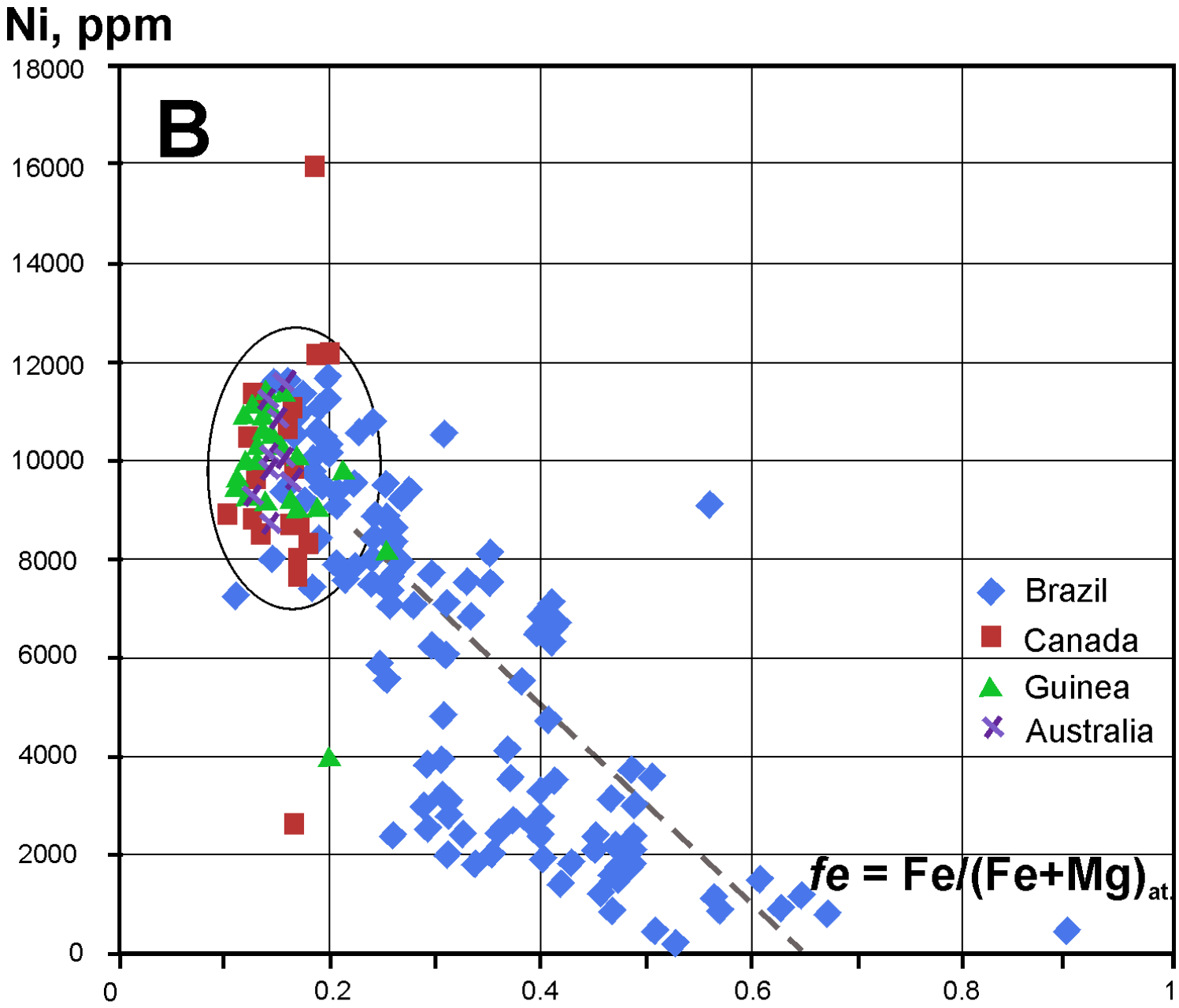

Figure 4B

This is a preprint, the final version is subject to change, of the American Mineralogist (MSA)
Cite as Authors (Year) Title. American Mineralogist, in press.
(DOI will not work until issue is live.) DOI: http://dx.doi.org/10.2138/am-2017-5949

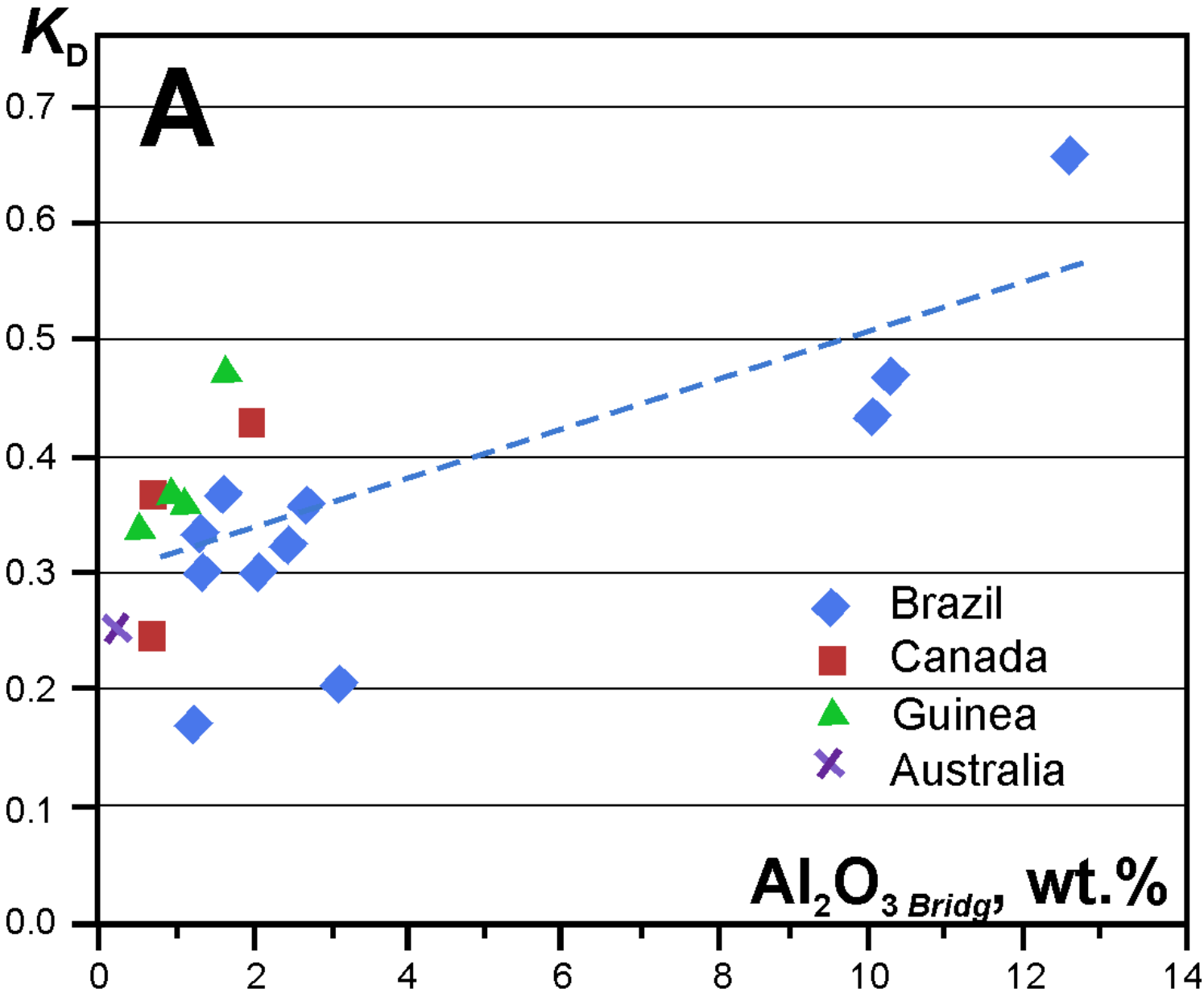

Figure 5A

This is a preprint, the final version is subject to change, of the American Mineralogist (MSA)
Cite as Authors (Year) Title. American Mineralogist, in press.
(DOI will not work until issue is live.) DOI: http://dx.doi.org/10.2138/am-2017-5949

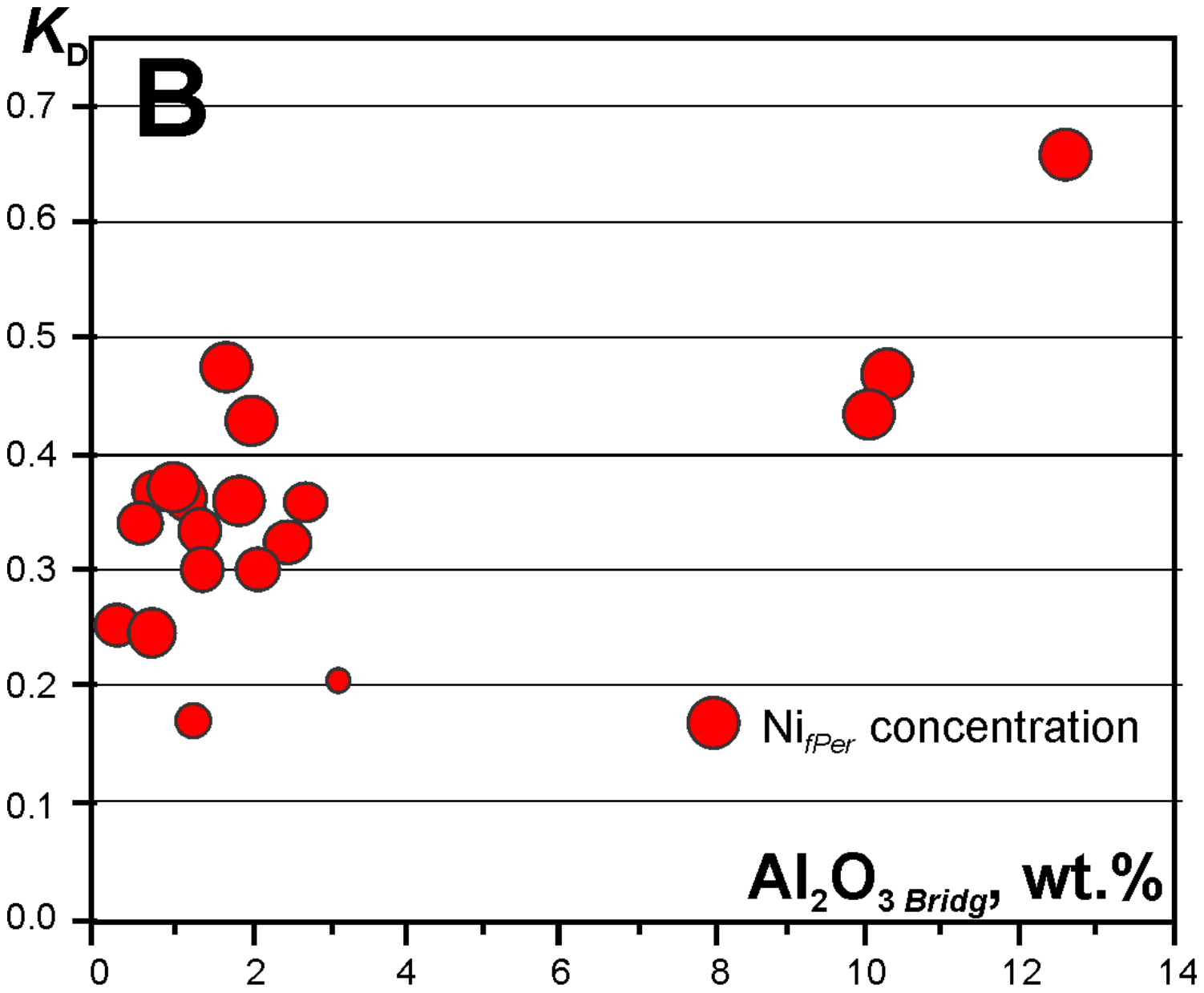

Figure 5B

This is a preprint, the final version is subject to change, of the American Mineralogist (MSA)
Cite as Authors (Year) Title. American Mineralogist, in press.
(DOI will not work until issue is live.) DOI: http://dx.doi.org/10.2138/am-2017-5949

Table 1

Sample #	Mg	Fe	Ni	Mn	Ca	Na	K	A_{total} (VIII/XII)	Si	Al	Ti	Cr	B_{total} (VI)	Refs*
Juina area, Brazil														
BZ120	0.878	0.064	0.000	0.002	0.001	0.002	0.000	0.948	0.943	0.024	0.003	0.006	0.976	1
BZ207	0.795	0.125	0.000	0.004	0.001	0.002	0.000	0.928	0.923	0.052	0.003	0.002	0.980	1
BZ210	0.750	0.071	0.000	0.013	0.012	0.034	0.006	0.885	0.856	0.197	0.000	0.016	1.069	1
BZ241	0.674	0.075	0.000	0.018	0.012	0.027	0.000	0.805	0.903	0.201	0.000	0.015	1.120	1
BZ242	0.406	0.055	0.000	0.018	0.078	0.149	0.000	0.707	0.915	0.247	0.000	0.023	1.185	1
BZ251	0.900	0.053	0.000	0.002	0.001	0.001	0.000	0.957	0.950	0.026	0.002	0.005	0.983	1
14-2	0.833	0.068	0.000	0.002	0.021	0.004	0.000	0.928	0.946	0.027	0.001	0.006	0.980	2
1-5	0.863	0.087	0.000	0.002	0.001	0.000	0.000	0.953	0.934	0.041	0.001	0.003	0.979	3
3-2	0.830	0.059	0.000	0.002	0.001	0.000	0.000	0.891	0.969	0.031	0.003	0.003	1.006	3
3-5	0.824	0.092	0.000	0.004	0.000	0.000	0.000	0.920	0.927	0.061	0.003	0.003	0.993	3
4-3	0.877	0.059	0.000	0.001	0.000	0.002	0.000	0.941	0.933	0.048	0.003	0.004	0.987	**3**
Northwest Territories, Canada														
DO2700100	0.940	0.040	0.000	0.001	0.007	0.000	0.000	0.988	0.956	0.014	0.000	0.004	0.973	4
DO2700300	0.938	0.041	0.000	0.001	0.001	0.002	0.000	0.984	0.981	0.014	0.000	0.004	0.998	4
DO27-97 14A	0.896	0.059	0.000	0.001	0.002	0.001	0.000	0.959	0.953	0.040	0.000	0.005	0.998	**4**
Kankan area, Guinea														
KK-103	0.891	0.047	0.000	0.001	0.001	0.001	0.000	0.942	0.955	0.012	0.000	0.002	0.970	5
KK-108	0.866	0.068	0.000	0.002	0.002	0.001	0.000	0.939	0.946	0.033	0.001	0.003	0.983	5
KK-16	0.892	0.046	0.000	0.002	0.001	0.002	0.000	0.943	0.957	0.011	0.000	0.004	0.972	5
KK-44	0.911	0.049	0.000	0.002	0.001	0.002	0.000	0.965	0.962	0.023	0.001	0.005	0.991	**5**
Eurelia area, South Australia														
FBS5-11	0.908	0.041	0.001	0.002	0.001	0.000	0.000	0.953	0.999	0.005	0.000	0.005	1.010	**6**

Note: *References: 1 – Hutchison (1997), 2 – Zedgenizov et al. (2014), 3 – Hayman et al. (2005), 4 - Davies et al. (2004), 5 – Stachel et al. (2000), 6 – Tappert et al. (2009).

This is a preprint, the final version is subject to change, of the American Mineralogist (MSA)
Cite as Authors (Year) Title. American Mineralogist, in press.
(DOI will not work until issue is live.) DOI: http://dx.doi.org/10.2138/am-2017-5949

Table 2

Sample #	Mineral association	Bridgmanite				Ferropericlase				$K_D^{Br\text{-}fPer}$	Refs**
		FeO, wt%	MgO, wt%	Al_2O_3, wt%	*fe*	FeO, wt%	MgO, wt%	Ni, ppm	*fe*		
Juina area, Brazil											
BZ120	Bridg+fPer	4.63	35.39	1.23	0.069	42.81	55.25	6052	0.310	0.1688	1
BZ207	Bridg+fPer+Jeffbenite	9.02	32.03	2.66	0.138	43.14	54.84	7074	0.313	0.3580	1
BZ210	Bridg+fPer	5.14	30.21	10.04	0.088	27.20	69.22	9982	0.183	0.4330	1
BZ241	Bridg+fPer+Ruby	5.36	27.15	10.24	0.101	28.63	68.21	11711	0.193	0.4704	1
BZ242	Bridg+fPer	3.95	16.35	12.58	0.120	25.50	69.30	11083	0.173	0.6566	1
BZ251	Bridg+fPer	3.80	36.25	1.33	0.056	23.52	74.77	9825	0.152	0.3332	1
14-2	Bridg+fPer+Di?	4.87	33.59	1.37	0.086	31.50	65.60	9746	0.216	0.3019	2
1-5	Bridg+fPer	6.25	34.80	2.07	0.093	36.70	60.98	9137	0.258	0.2982	3
3-2	Bridg+fPer+CaSiPv+'Ol'	4.21	33.43	1.60	0.066	25.27	72.21	10336	0.166	0.3599	3
3-5	Bridg+fPer+'Ol'	6.60	33.20	3.10	0.101	48.96	50.34	2437	0.363	0.2044	3
4-3	Bridg+fPer+'Ol'	4.27	35.36	2.45	0.064	25.67	71.11	10631	0.168	0.3810	3
Northwest Territories, Canada											
DO2700100	Bridg+fPer+CaSiPv+SiMg	2.85	37.90	0.69	0.041	16.80	81.60	8882	0.104	0.3652	4
DO2700300	Bridg+fPer+'Ol'	2.97	37.80	0.72	0.042	23.60	73.70	11083	0.154	0.2454	4
DO27-97 14A	Bridg+fPer+Ni	4.22	36.11	2.03	0.062	21.29	77.45	10742	0.135	0.4251	4
Kankan area, Guinea											
KK-103	Bridg+fPer	3.39	35.92	0.61	0.050	20.11	76.98	11004	0.129	0.3876	5
KK-108	Bridg+fPer+Ga	4.90	34.90	1.67	0.037	22.15	75.61	10049	0.143	0.4788	5
KK-16	Bridg+fPer+Siderite	3.34	35.94	0.55	0.050	22.68	75.34	11212	0.146	0.3425	5
KK-44	Bridg+fPer+CaSiPv+'Ol'	3.52	36.73	1.19	0.051	20.15	76.45	10532	0.130	0.3634	5
Eurelia area, South Australia											
FBS5-11	Bridg+fPer	2.93	36.58	0.25	0.043	23.42	74.04	9550	0.152	0.2532	6

Note: * Bridg: bridgmanite; fPer: ferropericlase; Di?: suggested diopside; CaSiPrv: CaSi-perovskite; 'Ol': phase with an olivine composition; SiMg: unidentified Si-Mg phase; Ni: native Ni; Ga: garnet.

** Reference numbers are the same as in Table 1.